CAMBRIDGE
UNIVERSITY PRESS

Article

The mineralogy of the historical Mochalin Log REE deposit, South Urals, Russia. Part I. New gatelite-group minerals ferriperbøeite-(La), $(CaLa_3)(Fe^{3+}Al_2Fe^{2+})[Si_2O_7][SiO_4]_3O(OH)_2$ and perbøeite-(La), $(CaLa_3)(Al_3Fe^{2+})[Si_2O_7][SiO_4]_3O(OH)_2$

Anatoly V. Kasatkin[1]* , Natalia V. Zubkova[2], Igor V. Pekov[2,3], Nikita V. Chukanov[4], Radek Škoda[5],
Yury S. Polekhovsky[6,†], Atali A. Agakhanov[1], Dmitriy I. Belakovskiy[1], Aleksey M. Kuznetsov[7], Sergey N. Britvin[6]
and Dmitry Yu. Pushcharovsky[2]

[1]Fersman Mineralogical Museum of the Russian Academy of Sciences, Leninsky Prospekt 18-2, 119071 Moscow, Russia; [2]Faculty of Geology, Moscow State University, Vorobievy Gory, 119991 Moscow, Russia; [3]Vernadsky Institute of Geochemistry and Analytical Chemistry, Russian Academy of Sciences, Kosygina str. 19, 119991 Moscow, Russia; [4]Institute of Problems of Chemical Physics, Russian Academy of Sciences, 142432 Chernogolovka, Moscow region, Russia; [5]Department of Geological Sciences, Faculty of Science, Masaryk University, Kotlářská 2, 611 37, Brno, Czech Republic; [6]Institute of Earth Sciences, St Petersburg State University, University Embankment 7/9, 199034 St Petersburg, Russia; and [7]Oktyabrskaya str., 5-337, 454071 Chelyabinsk, Russia

Abstract

The paper opens a series devoted to the mineral diversity of the Mochalin Log rare earth element (*REE*) deposit, South Urals, Russia. There is a brief outline of the history of studies and geology of the deposit as well as the description of two new isostructural gatelite-group minerals, ferriperbøeite-(La) $(CaLa_3)(Fe^{3+}Al_2Fe^{2+})[Si_2O_7][SiO_4]_3O(OH)_2$ and perbøeite-(La) $(CaLa_3)(Al_3Fe^{2+})[Si_2O_7][SiO_4]_3O(OH)_2$. Both minerals occur in polymineralic nodules and are associated with one another and allanite-(Ce), allanite-(La), bastnäsite-(Ce), bastnäsite-(La), ferriallanite-(Ce), ferriallanite-(La), ferriperbøeite-(Ce), perbøeite-(Ce), törnebohmite-(Ce) and törnebohmite-(La). The new minerals form isolated anhedral grains up to 0.3 mm [ferriperbøeite-(La)] and 0.5 mm [perbøeite-(La)] across and granular aggregates up to 1.5 mm × 0.5 mm [ferriperbøeite-(La)] and 3 mm × 1 mm [perbøeite-(La)]. Both minerals are brownish-black with vitreous lustre. $D_{calc} = 4.510$ [ferriperbøeite-(La)] and 4.483 [perbøeite-(La)] g cm^{-3}. They are optically biaxial (+); ferriperbøeite-(La): α = 1.788(5), β = 1.790(5), γ = 1.810(5) and $2V_{meas} = 40(10)°$; perbøeite-(La): α = 1.778(8), β = 1.783(8), γ = 1.805(8) and $2V_{meas} = 40(10)°$. Chemical data [wt.%, electron-microprobe; Fe^{3+}:Fe^{2+} ratio from charge-balance requirements, H$_2$O by stoichiometry; ferriperbøeite-(La)/perbøeite-(La)] are: CaO 4.91/4.81, ThO$_2$ 0.00/0.32, La$_2$O$_3$ 23.75/22.16, Ce$_2$O$_3$ 19.69/20.05, Pr$_2$O$_3$ 0.85/1.09, Nd$_2$O$_3$ 1.48/2.18, MgO 1.47/1.38, Al$_2$O$_3$ 10.68/11.25, MnO 1.07/0.92, FeO 3.04/3.35, Fe$_2$O$_3$ 5.31/3.78, TiO$_2$ 0.19/0.19, SiO$_2$ 27.47/27.35, F 0.11/0.23, H$_2$O 1.61/1.54, $-O = F$ $-0.05/-0.10$, total 101.58/100.50. The empirical formulae based on O$_{20}$(OH,F)$_2$ are for ferriperbøeite-(La): $(Ca_{0.95}La_{1.58}Ce_{1.30}Nd_{0.10}Pr_{0.06})_{\Sigma 3.99}(Al_{2.27}Fe^{3+}_{0.72}Fe^{2+}_{0.46}Mg_{0.40}Mn_{0.16}Ti_{0.03})_{\Sigma 4.04}Si_{4.96}O_{20}[(OH)_{1.94}F_{0.06}]$; and for perbøeite-(La): $(Ca_{0.94}Th_{0.01}La_{1.49}Ce_{1.34}Nd_{0.14}Pr_{0.07})_{\Sigma 3.99}(Al_{2.42}Fe^{3+}_{0.52}Fe^{2+}_{0.51}Mg_{0.38}Mn_{0.14}Ti_{0.03})_{\Sigma 4.00}Si_{4.99}O_{20}[(OH)_{1.87}F_{0.13}]$. Both minerals are monoclinic, $P2_1/m$; the unit-cell parameters [ferriperbøeite-(La)/perbøeite-(La)] are: $a = 8.9458(2)/8.9652(4)$, $b = 5.72971(13)/5.7306(2)$, $c = 17.6192(3)/17.6770(9)$ Å, β = 115.9497(19)/116.053(6)°, $V = 812.06(3)/815.88(6)$ Å^3 and $Z = 2/2$. The crystal structures are solved on a single crystal and converged to $R = 0.0355$ [ferriperbøeite-(La)] and 0.0750 [perbøeite-(La)]. Ferriperbøeite-(La) and perbøeite-(La) are named as the La-analogues of ferriperbøeite-(Ce) and perbøeite-(Ce), respectively.

Introduction

This article is the first in a series regarding new minerals with *REE* as species-defining cations (henceforth 'REE minerals') from polymineralic nodules found in the Mochalin Log deposit, Chelyabinsk Oblast, South Urals, Russia. The discoveries are the result of a focused study regarding the mineral diversity of this famous rare-earth deposit.

The Mochalin Log REE deposit:

Historical context

Due to its unique rare-earth mineralisation and rich species diversity, Mochalin Log is a famous mineral locality in the South Urals. It is located at 55°48′42″N, 60°33′46″E, in the valley

*Author for correspondence: Anatoly V. Kasatkin, E-mail: anatoly.kasatkin@gmail.com
†Deceased 28 September 2018.

Fig. 1. Geographical position of the Mochalin Log deposit.

of the Mochalin Log stream ('log' in Russian means 'large gentle ravine'), a tributary of the Borzovka river, in the Potaniny (Potaninskie) Mountains. It is ~10 km N of Kyshtym and ~90 km NNW of Chelyabinsk and 120 km S of Ekaterinburg (Fig. 1).

In the 19th century, the area was mined as a placer gold deposit and the first recorded *REE* mineral, 'kyshtymoparisite' (Korovaev, 1861) later recognised as a member of the bastnäsite group, was reported as early as 1861. By the beginning of the 20th century gold mining had ceased, but the unusual alluvial pebbles and nodules containing *REE* minerals were abundant on the mine dumps, and began to draw the attention of mineralogical researchers.

The earliest phase of research dates to the late 1920s when Mochalin Log was studied intensively by outstanding Russian mineralogist and geochemist Veniamin Arkadievich Silberminz (1887–1939) and his colleagues. They undertook a geological and petrological review of the deposit and provided detailed descriptions of the multiple dumps that contained significant nodules and numbered these dumps 1–8. The minerals bastnäsite, cerite, chevkinite, 'lessingite' (britholite), 'orthite' (allanite) and törnebohmite were identified (Silberminz, 1928, 1929, 1930; Alimarin, 1930; Knipovitch, 1930; Kuznetsov, 1930).

From the mid 1950s to mid 1960s the Uralian mineralogist Nikolay Vasilievich Svyazhin (1927–1967) focused on the deposit. He further described the mineralogy of the nodules, noting also 'cerianite' and providing improved physical and optical properties alongside chemical data. Of particular note are the reported ratios of Ce/La, OH/F and the first X-ray diffraction (XRD) data (Svyazhin, 1956, 1962, 1965a,b; Yunikov and Svyazhin, 1965).

At the turn of the 20th Century, one of the authors (I.V.P) focused his attention on the deposit, culminating in its attribution as type locality for two minerals, hydroxylbastnäsite-(Ce) (the 'kyshtymoparisite' reported by Silberminz in 1929) and

törnebohmite-(La) [a new species proposed by Levinson (1966) based on data from Svyazhin (1962)]. Furthermore, several nodules were analysed with electron microprobe techniques (EMPA) and powder XRD, providing important new data on the bastnäsite group and lanthanide composition in other *REE* minerals (Pekov *et al.*, 2002; Alimova *et al.*, 2003).

The current study was initiated in 2017 to focus on mineral species diversity at the locality and build on the work of those listed above. So far, 380 nodules have been investigated and 300 have been shown to contain *REE* minerals. All nodules have been studied using scanning electron microscopy (SEM) and EMPA, and grains separated from ~40 nodules have been investigated by other analytical methods including, but not limited to, single-crystal XRD, powder XRD, Raman and infrared (IR) spectroscopy. Selected results of these analyses are presented herein and in the accompanying series of articles to be published.

Geological context

The Mochalin Log deposit is related to the southern contact zone of the Vishnevogorskiy alkaline (syenite–miaskite) intrusive complex, this is composed mainly of miaskites, alkaline syenites and granite–gneisses with minor amphibolites (Fig. 2). The miaskites are typically composed of microcline, nepheline, albite and biotite (mainly annite, rarely Fe-enriched phlogopite) with accessory magnetite, rutile (Nb-enriched variety, so-called ilmenorutile), fluorapatite, titanite, zircon and secondary zeolites. In the peripheral parts of the bodies, these transition into alkaline syenites composed mainly of albite and microcline with alkali pyroxene and minor biotite, quartz and titanite. The alkaline syenites in turn transition into the granite–gneisses which occupy the central part of the Mochalin Log valley. They are composed of quartz, microcline, albite (including plagioclase with composition $Ab_{86}An_{14}$) and aegirine–augite with accessory fluorapatite, titanite and zircon. The rare amphibolites are composed of approximately equal amounts of plagioclase ($Ab_{70}An_{30}$) and amphibole-group minerals with very minor quartz, titanite, fluorapatite and diopside (Silberminz, 1930). The current work has incidentally identified that the amphiboles are represented by hornblende- (magnesio-hornblende, magnesio-ferri-hornblende and ferro-ferri-hornblende) and hastingsite- (hastingsite *ss*, magnesio-hastingsite, potassic-hastingsite and potassic-magnesio-hastingsite) series minerals.

The rich *REE* mineralisation, presented in nodules of the Mochalin Log placer deposit, has a contact metasomatic origin. Although not confirmed, it was probably formed during fenitisation of granitic pegmatites located within granite–gneisses in the exocontact zone of the alkaline intrusion of Potaniny Mts.

A detailed description of the geology and petrology of the deposit can be found elsewhere, such as Silberminz (1930), Kuznetsov (1930) and Svyazhin (1956).

Mineralogical context

The great diversity of *REE* minerals forming nodules are the outstanding mineralogical feature of the Mochalin Log deposit. Most nodules have been collected from dumps 2, 5, 7, 8 and in a dump hereby designated '2*bis*' that was uncovered in 2018 (Figs 2, S1). The typical nodule size is 1 to 7 cm (Fig. S2a) however, the biggest recorded was 12 cm across, weighing 2 kg (Silberminz, 1930). It is still possible to find large nodules and in 2019 one of the authors (A.M.K.) found at dump 7 a nodule measuring 11 cm × 10 cm × 6 cm, weighing 1.1 kg (Fig. S2b).
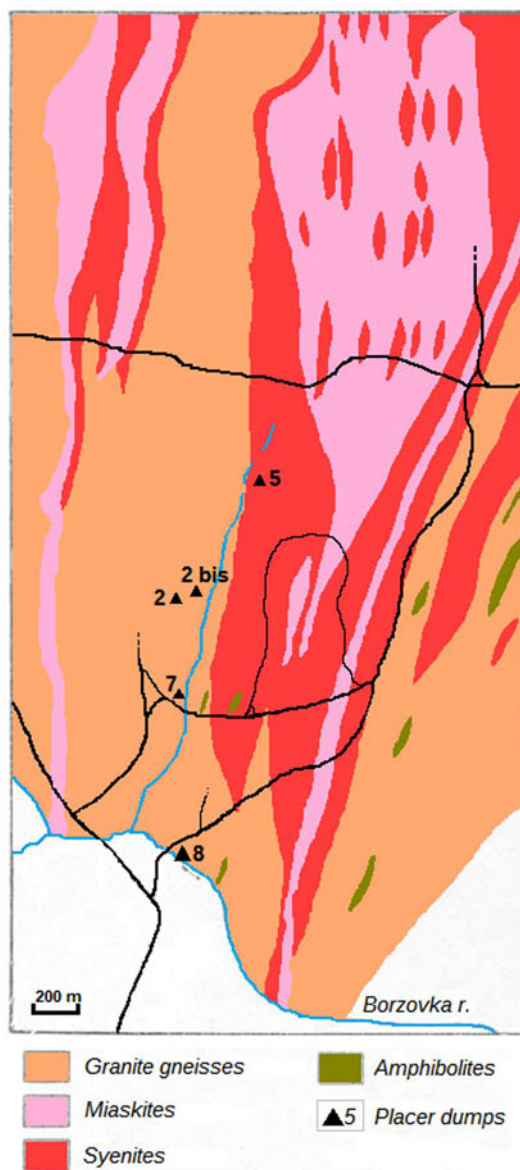
Fig. 2. Geological map of the Mochalin Log deposit (modified after Kuznetsov, 1930).

Thirty-seven *REE* mineral species have been identified from Mochalin Log for the first time during our works, eight of which are new to science and have been approved by the Commission on New Minerals, Nomenclature and Classification (CNMNC) of the International Mineralogical Association (IMA), two of those being the focus of the latter part of this article. This brings the total of all recognised *REE* minerals at the deposit to 51. Alongside species identification, the frequency of species occurrence in the 300 *REE*-bearing nodules studied has been noted and rated; abundant ($n > 100$ nodule occurrences), common ($n = 50$–99), subordinate ($n = 20$–49), rare ($n = 5$–19) and very rare ($n < 5$). An overview of this data gathering exercise is presented in Table 1.

Each nodule typically contains several *REE* minerals, 8 to 15 distinct species is common but as many as 21 have been found. Monomineralic nodules are very rare, only four were identified composed completely of bastnäsite-(Ce), bastnäsite-(La), ferriallanite-(Ce) and perrierite-(Ce). Previously, Alimova *et al.* (2003) recorded several monomineralic allanite nodules.

Associated non-*REE* minerals in these nodules are numerous but usually very minor by volume. The full list of these species and their distribution in the 300 *REE* nodules studied, using the same scale as for *REE* minerals, are given in Supplementary material (Table S1).

Regarding general distribution of *REE* in the nodules, La and Ce significantly dominate other light rare earth elements (*LREE*) detectable by EPMA that shows Nd > Pr > Sm. In general, nodules show very steep *LREE* enrichment followed by heavy rare earth element (*HREE*) impoverishment in chondrite-normalised *REE* patterns. Four 'very rare' ($n = 1$) species were identified with a *REE* dominance other than La or Ce, aeschynite-(Nd), aeschynite-(Y), fergusonite-(Y) and xenotime-(Y). All were found in nodules composed dominantly of the non-*REE* minerals albite, microcline and quartz, so it is suggested these represent a different assemblage with a paragenesis related to the common granitic pegmatites.

The gross La:Ce ratio varies widely from one nodule to another but is often close to 1:1, therefore both Ce- and La-dominant members of the same mineral series or group may occur in the same specimen, examples include, allanite, bastnäsite, ferri-allanite, monazite and perrierite and the later focus of this paper, ferriperbøeite and perbøeite. It should be noted that the absence of a 'Levinson suffix' in the text below should be interpreted as the presence of both Ce- and La-dominant mineral species together.

A significant exception to this is fluorbritholite, which was 'abundant' ($n > 100$), yet only twice showed a slight dominance of La over Ce, but not enough to consistently characterise what would be the new mineral species 'fluorbritholite-(La)'. Even in the nodules where all other *REE* minerals are La-dominant, fluorbritholite showed Ce >> La.

The *REE*-bearing nodules can be divided into two main types on the basis of their internal textures. Type 1 shows concentric zonation and are typically ovoid, the core is bastnäsite, an intermediate zone is perbøeite/ferriperbøeite and/or törnebohmite and/or fluorbritholite-(Ce) while the rim is allanite/ferriallanite (Fig. 3). The ovoid structures were reported previously (e.g. Silberminz, 1930; Svyazhin, 1956; Alimova *et al.*, 2003) and while these works mention identical core (bastnäsite) and rim (allanite) minerals, the middle zone is mainly reported as cerite-(Ce), which in the literature is reported as a common mineral from the locality (Silberminz, 1928, 1929, 1930; Yunikov and Svyazhin, 1965). This is in direct contradiction with results presented herein, where cerite-(Ce) was found in only two nodules.

In type 2 nodules, *REE* minerals form thin and chaotic intergrowths with each other, typically composed of allanite/ferriallanite, bastnäsite, fluorbritholite-(Ce), monazite, perbøeite/ferriperbøeite, perrierite and törnebohmite (Fig. 4).

Mochalin Log shows a similarity to the Bastnäs-type deposits at Riddarhyttan, Västmanland, Sweden (Öhman *et al.*, 2004; Holtstam and Andersson, 2007) and Jamestown, Colorado, USA (Allaz *et al.*, 2015), but has much greater *REE* mineral species diversity; it should be noted that all these occurrences differ in their attributed origin.

Ferriperbøeite-(La) and perbøeite-(La)

Ferriperbøeite-(La) [Russian Cyrillic: феррипербёит-(La)], ideally $(CaLa_3)(Fe^{3+}Al_2Fe^{2+})[Si_2O_7][SiO_4]_3O(OH)_2$, and perbøeite-(La) [Russian Cyrillic: пербёит-(La)], ideally $(CaLa_3)(Al_3Fe^{2+})[Si_2O_7][SiO_4]_3O(OH)_2$ are named in accordance with the gatelite supergroup nomenclature scheme (Bonazzi *et al.*, 2019) as analogues of

Table 1. REE minerals of the Mochalin Log deposit and their distribution (based on our data).

Mineral species	Simplified formula*	Distribution
Oxides		
Aeschynite-(Ce)**	$(Ce,Ca,Th)(Ti,Nb)_2(O,OH)_6$	X
Aeschynite-(Nd)**	$(Nd,Ln,Ca)(Ti,Nb)_2(O,OH)_6$	X
Aeschynite-(Y)**	$(Y,Ln,Ca,Th)(Ti,Nb)_2(O,OH)_6$	X
Cerianite-(Ce)[1]	CeO_2	XXXX
Fergusonite-(Y)**	$YNbO_4$	X
Nöggerathite-(Ce)**	$(Ce,Ca)_2Zr_2(Nb,Ti)(Ti,Nb)_2Fe^{2+}O_{14}$	X
Carbonates		
Ancylite-(Ce)**	$CeSr(CO_3)_2(OH)\cdot H_2O$	X
Bastnäsite-(Ce)[1]	$Ce(CO_3)F$	XXXXX
Bastnäsite-(La)[1]	$La(CO_3)F$	XXXXX
Calcioancylite-(Ce)**[1]	$(Ce,Ca,Sr)(CO_3)(OH,H_2O)$	X
Hydroxylbastnäsite-(Ce)[1]	$Ce(CO_3)(OH)$	XXX
Lanthanite-(La)**[1]	$La_2(CO_3)_3\cdot 8H_2O$	XXX
Parisite-(Ce)**	$CaCe_2(CO_3)_3F_2$	X
Synchysite-(Ce)**	$CaCe(CO_3)_2F$	X
Phosphates		
Florencite-(Ce)**	$CeAl_3(PO_4)_2(OH)_6$	X
Monazite-(Ce)[1]	$Ce(PO_4)$	XXXX
Monazite-(La)[1]	$La(PO_4)$	XXXX
Rhabdophane-(La)**[1]	$La(PO_4)\cdot H_2O$	X
Xenotime-(Y)**	$Y(PO_4)$	X
Silicates		
Alexkuznetsovite-(La) [IMA 2019–081][1]	$La_2Mn(Si_2O_7)(CO_3)$	XX
Alexkuznetsovite-(Ce) [IMA 2019–118][1]	$Ce_2Mn(Si_2O_7)(CO_3)$	XX
Allanite-(Ce)[1]	$(CaCe)(Al_2Fe^{2+})[Si_2O_7][SiO_4]O(OH)$	XXXXX
Allanite-(La)[1]	$(CaLa)(Al_2Fe^{2+})[Si_2O_7][SiO_4]O(OH)$	XXXX
Biraite-(Ce)**[1]	$Ce_2Fe^{2+}(Si_2O_7)(CO_3)$	XX
Biraite-(La) [IMA2020-020]	$La_2Fe^{2+}(Si_2O_7)(CO_3)$	XX
Britholite-(Ce)?	$(Ce,Ca)_5(SiO_4)_3(OH)$	
Cerite-(Ce)	$(Ce,La,Ca)_9(Mg,Fe^{3+})(SiO_4)_3(SiO_3OH)_4(OH)_3$	X[$]
Chevkinite-(Ce)?	$Ce_4(Ti,Fe^{2+},Fe^{3+})_5O_8(Si_2O_7)_2$	
Christofschäferite-(Ce)**[1]	$(Ce,La,Ca)_4Mn(Ti,Fe)_3(Fe,Ti)(Si_2O_7)_2O_8$	X
Dingdaohengite-(Ce)**[1]	$(Ce,La)_4Fe^{2+}(Ti,Fe^{2+},Mg,Fe^{3+})_2Ti_2Si_4O_{22}$	X
Dissakisite-(Ce)**[1]	$CaCe(Al_2Mg)[Si_2O_7][SiO_4]O(OH)$	X
Dissakisite-(La)**[1]	$CaLa(Al_2Mg)[Si_2O_7][SiO_4]O(OH)$	XX
Ferriallanite-(Ce)**[1]	$(CaCe)(Fe^{3+}AlFe^{2+})[Si_2O_7][SiO_4]O(OH)$	XXXXX
Ferriallanite-(La)**[1]	$(CaLa)(Fe^{3+}AlFe^{2+})[Si_2O_7][SiO_4]O(OH)$	XXXX
Ferriperbøeite-(Ce)**[1]	$(CaCe_3)(Fe^{3+}Al_2Fe^{2+})[Si_2O_7][SiO_4]_3O(OH)_2$	XXXX
Ferriperbøeite-(La) [IMA 2018–106]	$(CaLa_3)(Fe^{3+}Al_2Fe^{2+})[Si_2O_7][SiO_4]_3O(OH)_2$	XXXX
Fluorbritholite-(Ce)**[1]	$(Ce,Ca)_5(SiO_4)_3F$	XXXXX
Gadolinite-(Ce)?	$Ce_2Fe^{2+}Be_2O_2(SiO_4)_2$	
Gatelite-(Ce)**[1]	$(Ca,Ce)_4(Al,Mg,Fe)_4(Si_2O_7)(SiO_4)_3(O,F,OH)_3$	XX
Perbøeite-(Ce)**[1]	$(CaCe_3)(Al_3Fe^{2+})[Si_2O_7][SiO_4]_3O(OH)_2$	XXX
Perbøeite-(La) [IMA 2018–116]	$(CaLa_3)(Al_3Fe^{2+})[Si_2O_7][SiO_4]_3O(OH)_2$	XXXX
Percleveite-(Ce)**[1]	$Ce_2Si_2O_7$	XX
Percleveite-(La) [IMA 2019–037][1]	$La_2Si_2O_7$	XX
Perrierite-(Ce)**[1]	$Ce_4MgFe^{3+}_2Ti_2O_8(Si_2O_7)_2$	XXXX
Perrierite-(La)**[1]	$(La,Ce,Ca)_4(Fe^{2+},Mn)(Ti,Fe^{3+},Al)_4[(Si_2O_7)O_4]_2$	XXX
Radekškodaite-(Ce) [IMA 2019–042][1]	$(CaCe_5)(Al_4Fe^{2+})[Si_2O_7][SiO_4]_5O(OH)_3$	X
Radekškodaite-(La) [IMA 2018–107][1]	$(CaLa_5)(Al_4Fe^{2+})[Si_2O_7][SiO_4]_5O(OH)_3$	XX
Stetindite-(Ce)**[1]	$Ce^{4+}(SiO_4)$	XX
Stillwellite-(Ce)**	$CeBSiO_5$	X
Törnebohmite-(Ce)[1]	$Ce_2Al(SiO_4)_2(OH)$	XXXX
Törnebohmite-(La)[1]	$La_2Al(SiO_4)_2(OH)$	XXXXX

Notes: Distribution of minerals: XXXXX – abundant, XXXX – common, XXX – subordinate, XX – rare, X – very rare.
Minerals for which Mochalin Log deposit is type locality are given in *italic*. Those of them that are discovered by us are given in ***bold italic*** with IMA numbers in square brackets.
*Formulae are given in accordance with the New IMA List of Minerals (Pasero, 2020).
**Minerals identified by the authors for the first time at the deposit.
[$]According to our data; in the literature, however, cerite-(Ce) is mentioned as common (Silberminz, 1928, 1929, 1930; Yunikov and Svyazhin, 1965).
? Mineral is mentioned in the literature but its identification remains questionable.
[1]Minerals associated with ferriperboeite-(La) and perboeite-(La).

ferriperbøeite-(Ce) (Bindi et al., 2018) and perbøeite-(Ce) (Bonazzi et al., 2014), respectively, with La as the dominant REE.

Both new minerals and their names have been approved by the IMA-CNMNC as IMA2018-106 [ferriperbøeite-(La), Kasatkin et al., 2018] and IMA2018-116 [perbøeite-(La), Kasatkin et al., 2019]. The holotype specimens are deposited in the systematic collection of the Fersman Mineralogical Museum of the Russian Academy of Sciences, Moscow with the catalogue numbers 96276 [ferriperbøeite-(La)] and 96484 [perbøeite-(La)].

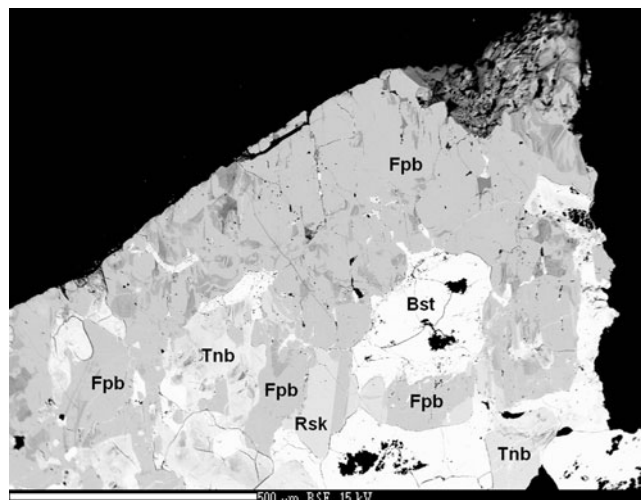### Occurrence and general appearance

Nodules containing both new minerals were first found in 1980s by local collectors at dump no. 2 (Fig. S1a) and preserved in the

Fig. 3. Cut and polished nodule showing typical ovoidal structure: orange-yellow core of bastnäsite (Bst), black middle zone of perbøeite/ferriperbøeite (Prb) and black rim of allanite/ferriallanite (Aln). Size of the sample: 2 cm × 1.7 cm. Photo: A.M. Kuznetsov, specimen no. ML 59-2.

Fig. 5. Ferriperbøeite-(La) (Fpb) associated with bastnäsite-(Ce) (Bst), törnebohmite-(La) (Tnb) and radekškodaite-(La) (Rsk). Dark-grey inclusions in ferriperbøeite-(La) are allanite-(La)/ferriallanite-(La). Black grains are quartz. In the right upper corner there is a trace from the grain extracted for the structural investigation. Polished section. SEM (back-scattered electron) image, scale bar 500 μm, specimen no. ML 56-2.

private collection of one of the authors (A.M.K.). In 2017 the specimens were cut, polished and given to the senior author (A.V.K.) for routine EMPA. This revealed two, then potentially new, *REE* minerals and started the characterisation and systematic study of the *REE* species diversity at Mochalin Log.

Ferriperbøeite-(La) and perbøeite-(La) occur in the polymineralic nodules composed mainly of bastnäsite, allanite/ferriallanite and törnebohmite (Figs 3–7). Each new mineral forms isolated anhedral grains, up to 0.3 mm for ferriperbøeite-(La) and 0.5 mm for perbøeite-(La), and granular aggregates, up to 1.5 mm × 0.5 mm for ferriperbøeite-(La) and 3 mm × 1 mm for perbøeite-(La). The nodules often have a concentrically zoned, ovoid structure with a core of bastnäsite, an intermediate zone of ferriperbøeite-(La)/perbøeite-(La) and a rim of allanite/

ferriallanite (Figs 3, 7). The new minerals are typically intimately intergrown with, or overgrown by törnebohmite and when aggregated contain inclusions of allanite/ferriallanite.

Ferriperbøeite-(La) and perbøeite-(La) should be considered 'common' minerals at Mochalin Log (Table 1), during this study, ferriperbøeite-(La) was found without perbøeite-(La) in 42 nodules, perbøeite-(La) was found without ferriperbøeite-(La) in 39 and the two minerals were found together in another 40; most of these nodules were from dumps nos. 2, 2*bis* and 7.

Ferriperbøeite-(La) and perbøeite-(La) occur in an assemblage rich in *REE* minerals. Apart from the texturally dominant species mentioned above, associated minerals also include 25
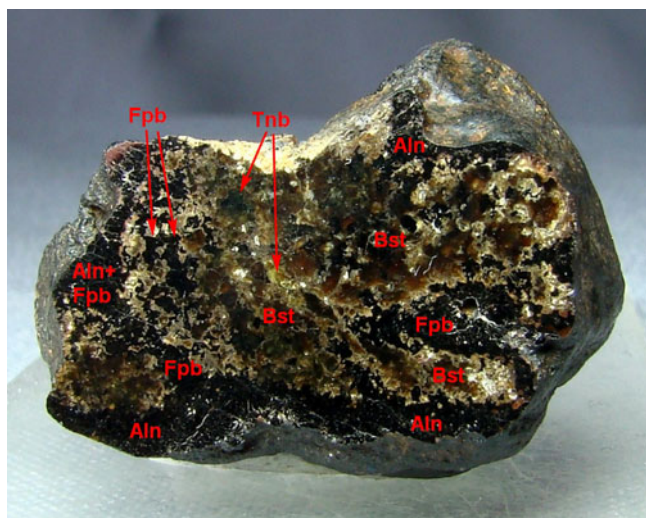
Fig. 4. Cut and polished section of nodule showing black ferriperbøeite-(La) (Fpb) intergrown with black allanite/ferriallanite (Aln), yellow and brown bastnäsite (Bst) and greenish to yellow-greenish törnebohmite (Tnb). Size of the nodule: 2.2 cm × 1.3 cm. Photo: A.M. Kuznetsov, specimen no. ML 56-2.
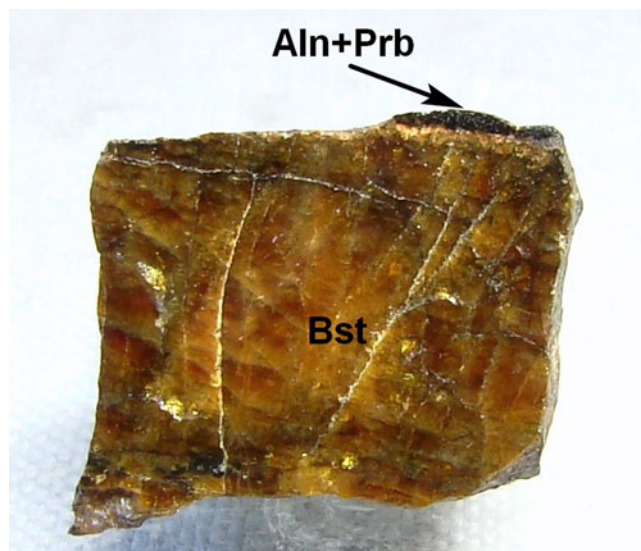
Fig. 6. Cut and polished section of nodule (fragment) showing thin black crust of perbøeite-(La) (Prb) together with allanite-(La)/ferriallanite-(La) (Aln) (see Fig. 7) on orange-yellow bastnäsite (Bst). Size of the sample: 1.5 cm × 1 cm. Photo: A.M. Kuznetsov, specimen no. ML 24-2.
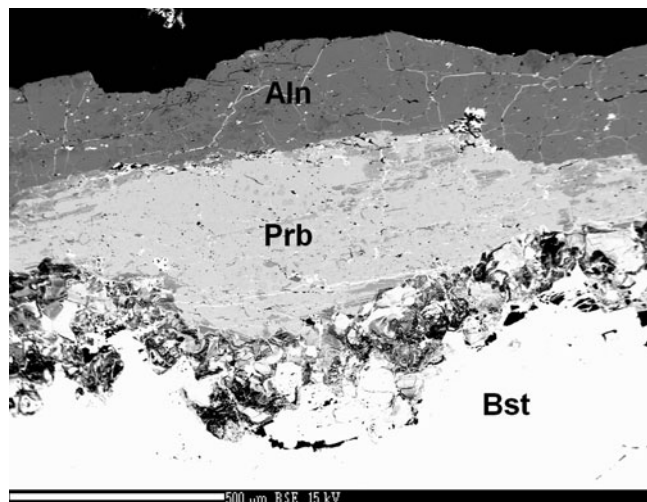
Fig. 7. Section of a crust (see Fig. 6) mainly consisting of perbøeite-(La) (Prb) which is 'sandwiched' between a bastnäsite-(Ce) core (Bst) and allanite-(La)/ferriallanite-(La) rim (Aln). Dark-grey inclusions in perbøeite-(La) are allanite-(La)/ferriallanite-(La), black grains are quartz. Polished section. SEM (back-scattered electron) image, scale bar 500 µm, specimen no. ML 24-2.

other *REE* minerals, two non-*REE* minerals that are in this case *REE*-bearing (huttonite and epidote), and 19 other non-*REE* minerals. All of these are marked with [1] symbol in Tables 1 and S1.

Physical properties and optical data

Both new minerals are brownish-black, translucent in thin fragments with brown streak and vitreous lustre. They are non-fluorescent under ultraviolet light. Both are brittle, cleavage is good on {100} and imperfect on {001}, parting is not observed and fracture is uneven (observed under the scanning electron microscope). Their Mohs' hardness is ~6, based on scratch tests. Their density could not be measured due to lack of pure material in suitable grains, so density values were calculated as 4.510 g cm^{-3} for ferriperbøeite-(La) and 4.483 g cm^{-3} for perbøeite-(La) using the empirical formulae and the unit-cell parameters from single-crystal XRD data.

Both minerals are optically biaxial (+). Ferriperbøeite-(La) has $\alpha = 1.788(5)$, $\beta = 1.790(5)$, $\gamma = 1.810(5)$ (589 nm), $2V_{meas} = 40(10)°$ and $2V_{calc} = 35°$. Dispersion of optical axes was not observed. The mineral is weakly pleochroic from nearly colourless in thin grains or pale-brownish in thicker ones (X) to greenish-brown (Y and Z). The absorption scheme is $Z > Y > X$. Perbøeite-(La) has $\alpha = 1.778(8)$, $\beta = 1.783(8)$, $\gamma = 1.805(8)$ (589 nm), $2V_{meas} = 40(10)°$ and $2V_{calc} = 51.5°$. Dispersion of optical axes is noticeable, inclined. Perbøeite-(La) is strongly pleochroic: X = colourless, Y = medium-dark brown, Z = nearly colourless or brownish. The absorption scheme is $Y > Z \sim X$. the optical orientation could not be determined for either mineral due to the anhedral shape of their grains.

In reflected light, both minerals are dark grey, anisotropy is weak for ferriperbøeite-(La) and very weak for perbøeite-(La). Bireflectance is very weak, $\Delta R = 0.5\%$ for ferriperbøeite-(La) and 0.3% (589 nm) for perbøeite-(La). The reflectance values, (R_{max}/R_{min}) for both minerals are given in Table 2, and were measured in air using a MSF-21 microspectrophotometer (LOMO company, St. Petersburg, Russia) with a monochromator slit width of 0.4 mm, beam diameter of 0.1 mm and SiC (474251, No. 545, Germany) used as a standard.

Table 2. Reflectance data (R, %) of ferriperbøeite-(La) [1] and perbøeite-(La) [2].

	[1]		[2]			[1]		[2]	
λ (nm)	R_{max}	R_{min}	R_{max}	R_{min}	λ (nm)	R_{max}	R_{min}	R_{max}	R_{min}
400	8.7	8.3	8.9	8.6	560	8.4	7.9	8.3	8.1
420	8.7	8.2	8.8	8.5	580	8.3	7.8	8.3	8.0
440	8.6	8.1	8.7	8.4	**589**	**8.3**	**7.8**	**8.3**	**8.0**
460	8.5	8.0	8.6	8.3	600	8.3	7.8	8.2	8.0
470	**8.5**	**8.0**	**8.6**	**8.3**	620	8.3	7.8	8.2	7.9
480	8.5	8.0	8.5	8.3	640	8.3	7.8	8.1	7.9
500	8.4	7.9	8.5	8.2	**650**	**8.3**	**7.8**	**8.1**	**7.9**
520	8.4	7.9	8.4	8.1	660	8.3	7.8	8.1	7.8
540	8.4	7.9	8.4	8.1	680	8.4	7.8	8.1	7.8
546	**8.4**	**7.9**	**8.4**	**8.1**	700	8.4	7.9	8.1	7.8

Data for wavelengths recommended by the IMA Commission on ore microscopy (COM) are marked in boldtype.

Neither mineral reacted with cold hydrochloric or nitric acid.

Raman spectroscopy

The Raman spectra (Figs 8 and 9) of ferriperbøeite-(La) and perbøeite-(La) were obtained from polished sections using a Horiba Labram HR Evolution spectrometer. This dispersive, edge-filter-based system is equipped with an Olympus BX 41 optical microscope, a diffraction grating with 600 grooves per millimetre, and a Peltier-cooled, Si-based charge-coupled device (CCD) detector. After careful tests with different lasers (473, 532 and 633 nm), the 633 nm He–Ne laser with the beam power of 10 mW at the sample surface was selected for acquisition to minimise analytical artefacts. The Raman signal was collected in the range of 100–4000 cm^{-1} with a 100× objective and the system being operated in confocal mode, beam diameter was ~1 µm and the lateral resolution ~2 µm. No visual damage of the analysed surface was observed at these conditions after the excitation. Wavenumber calibration was done using the Rayleigh line and low-pressure Ne-discharge lamp emissions. The wavenumber accuracy was ~0.5 cm^{-1}, and the spectral resolution was ~2 cm^{-1}. Band fitting was done after appropriate background correction, assuming combined Lorentzian-Gaussian band shapes using the Voigt function (*PeakFit*, Jandel Scientific Software).

The spectra of both minerals are very similar. Bands in the 3200–3350 cm^{-1} area correspond to O–H stretching vibrations of the O10–H and O11–H groups. The assignment of each band to a particular group is difficult, as the angle $\angle(D–H\cdots A)$ and the distance $D\cdots A$ contribute with opposite signs to the difference in the energies of hydrogen bonds formed by these groups (see structural data below). It is to be noted that correlations between wavenumbers of O–H stretching vibrations and lengths of hydrogen bonds (Libowitzky, 1999) cannot be applied to compare situations with significantly different $D\cdots H\cdots A$ angles. The ill-defined shoulder at 3437 cm^{-1} in the Raman spectrum of perbøeite-(La) could be due to adsorbed water or (taking into account minor amounts of Fe in the $M2$ site) O–H-stretching vibrations of the Fe$\cdots$O–H$\cdots$O fragments. Bands and shoulders in the 1000–1100 cm^{-1} range correspond to stretching vibrations of the Si–O–Si fragments in Si$_2$O$_7$ groups, those in the 850–1000 cm^{-1} region, to stretching vibrations of apical Si–O bonds, and those in the 660–700 cm^{-1} area to Al–O$\cdots$H bending vibrations. Bands in the 300–630 cm^{-1} range are due to mixed modes and overlapping bands of Al–O and Fe^{3+}–O stretching vibrations, as well as bending vibrations of silicate groups, while those with frequencies lower than
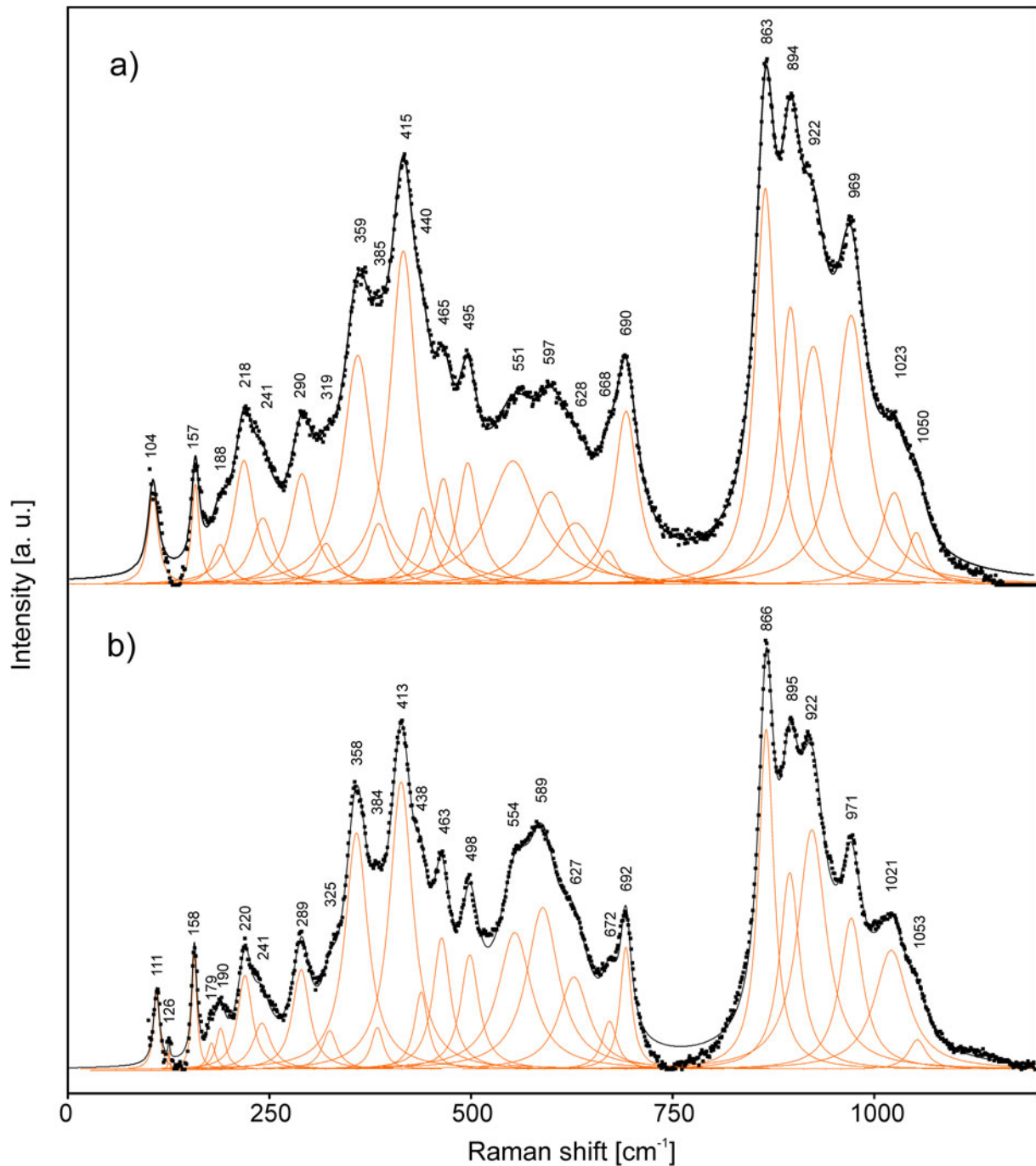
Fig. 8. Raman spectra of perbøeite-(La) (*a*) and ferriperbøeite-(La) (*b*) in the 100–1250 cm^{-1} region. The measured spectra are shown by dots. The curves matched to dots are a result of spectral fit as a sum of individual Voigt peaks shown below the curves.

300 cm^{-1} correspond to lattice modes involving *REE*–O-, Ca–O- and Fe^{2+}–O-stretching vibrations and librational vibrations of silicate groups. The Raman spectra of ferriperbøeite-(La) and perbøeite-(La) are similar to that of västmanlandite-(Ce) (Holtstam *et al.*, 2005) in the range of 300–1100 cm^{-1} but significantly differ from the latter in the regions of O–H stretching vibrations (above 3200 cm^{-1}) and stretching vibrations involving *REE* and divalent cations forming low-force-strength bonds (below 300 cm^{-1}).

The bands at 971, 692 and 413 cm^{-1} in the Raman spectrum of ferriperbøeite-(La) and those at 969, 690 and 415 cm^{-1} in the

Raman spectrum of perbøeite-(La) are close to strong bands in the Raman spectrum of allanite-(Ce) observed at 972, 689 and 421 cm^{-1} (Andò and Garzanti, 2014; Čopjaková *et al.*, 2015) and can be assigned tentatively to the epidote-type module (see below).

Infrared spectroscopy

Due to a lack of sizeable pure material, an IR absorption spectrum of perbøeite-(La) could not be obtained, and a spectrum for ferriperbøeite-(La) (Fig. 10) was obtained only after subtracting contributions from ferriallanite-(La) using a pure
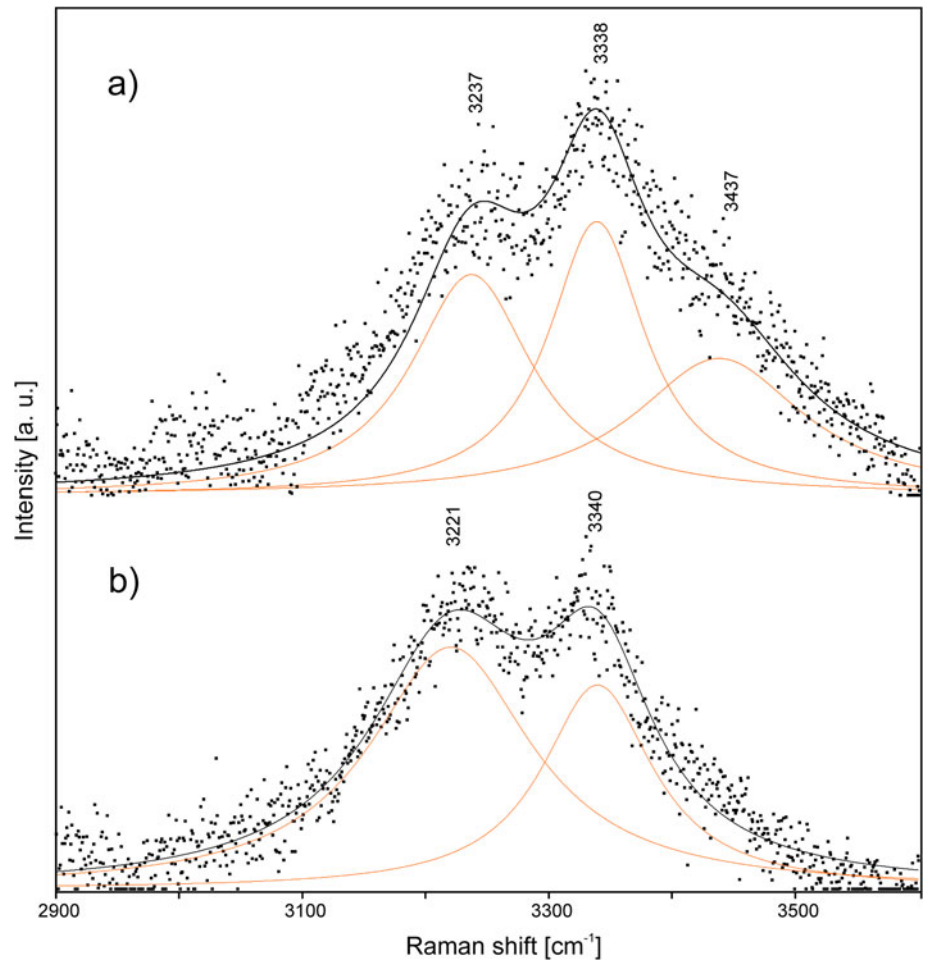
Fig. 9. Raman spectra of perbøeite-(La) (*a*) and ferriperbøeite-(La) (*b*) in the 2900–3600 cm^{-1} region. The measured spectra are shown by dots. The curves matched to dots are a result of spectral fit as a sum of individual Voigt peaks shown below the curves.

ferriallanite-(La) standard from the same assemblage as a comparator. Hand-picked fragments, ultimately composed of both ferriallanite-(La) and ferriperbøeite-(La) were ground in an agate mortar and pestle, mixed with anhydrous KBr, pelletised,

and analysed using an ALPHA FTIR spectrometer (Bruker Optics) in the range of wavenumbers from 360 to 3800 cm^{-1}, with a spectral resolution of 4 cm^{-1}. The IR spectrum of a pure KBr disk was used as a reference.
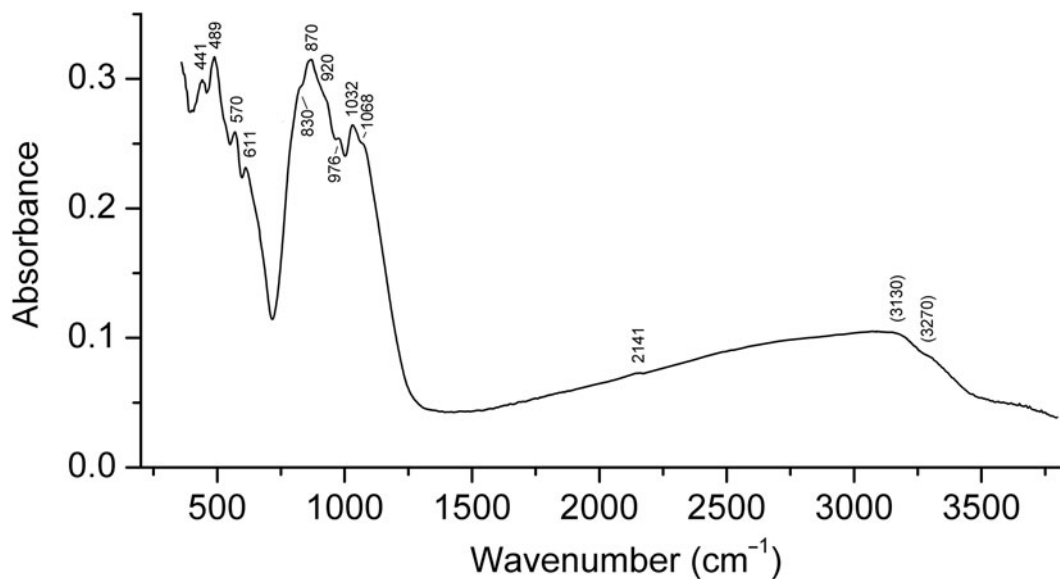
Fig. 10. Infrared absorption spectrum of ferriperbøeite-(La).

Table 3. Average chemical composition of ferriperbøeite-(La) and perbøeite-(La) (wt.%).

Constituent	Ferriperbøeite-(La) Mean, $n = 10$	Range	S.D.	Perbøeite-(La) Mean, $n = 10$	Range	S.D.	Probe standard
CaO	4.91	4.81–4.95	0.05	4.81	4.65–5.47	0.27	Wollastonite
La$_2$O$_3$	23.75	22.88–24.86	0.66	22.16	20.67–22.84	0.93	LaPO$_4$
Ce$_2$O$_3$	19.69	18.75–19.95	0.40	20.05	18.70–20.44	0.54	CePO$_4$
Pr$_2$O$_3$	0.85	0.73–0.93	0.08	1.09	0.91–1.17	0.10	PrPO$_4$
Nd$_2$O$_3$	1.48	1.19–1.78	0.21	2.18	1.55–2.47	0.31	NdPO$_4$
ThO$_2$	–			0.32	0.26–0.36	0.04	CaTh(PO$_4$)$_2$
MgO	1.47	1.38–1.55		1.38	1.17–1.50	0.12	Mg$_2$SiO$_4$
Al$_2$O$_3$	10.68	10.04–11.01	0.40	11.25	10.55–11.99	0.60	Sanidine
MnO	1.07	0.94–1.18	0.09	0.92	0.62–1.06	0.18	Spessartine
FeO*	3.04	7.18–8.06**	0.30**	3.35	6.01–6.77**	0.30**	Almandine
Fe$_2$O$_3$*	5.31			3.78			
TiO$_2$	0.19	0.14–0.24	0.03	0.19	0.08–0.34	0.09	Anatase Hardangervida
SiO$_2$	27.47	27.33–27.82	0.16	27.35	26.80–27.59	0.24	Sanidine
F	0.11	0.07–0.17	0.04	0.23	0.15–0.39	0.08	Topaz
H$_2$O$^\$$	1.61			1.54			
–O = F	–0.05			–0.10			
Total	101.58			100.50			

S.D. = standard deviation
*Apportioned from total Fe measured as FeO content of 7.82 wt.% for ferriperbøeite-(La) and 6.75 wt.% for perbøeite-(La) in accordance with bond-valence sums for the cationic sites and charge-balance requirement for the empirical formulae.
**For total iron calculated as FeO.
$^\$$Calculated by stoichiometry.
'–' = content of a constituent is below the detection limit.

Due to a rather strong scattering in the high-frequency region, bands of O–H-stretching vibrations are indistinct and could be determined only approximately (as a broad absorption band at ~3130 cm^{-1} and a shoulder at ~3270 cm^{-1}). The assignment of other IR absorption bands is as follows. Bands in 1000–1100 cm^{-1} area correspond to stretching vibrations of Si–O–Si fragments in Si$_2$O$_7$ groups, those in the 830–1000 cm^{-1} region, to stretching vibrations of apical Si–O bonds and, finally, those in the range of

Table 4. Crystal data, data collection information and structure refinement details for ferriperbøeite-(La) and perbøeite-(La).

Crystal data

Mineral	Ferriperbøeite-(La)	Perbøeite-(La)
Formula (species-defining elements are given in **bold**)	^{A1}(Ca$_{0.97}$LREE$_{0.03}$)$^{A2-4}$REE$_3$ ^{M1}(**Fe^{3+}**$_{0.44}$Al$_{0.36}$Mg$_{0.20}$) ^{M2}(**Al$_{1.90}$**Fe^{3+}$_{0.10}$)^{M3}(**Fe^{2+}**$_{0.46}$Mg$_{0.22}$Fe^{3+}$_{0.17}$Mn$_{0.15}$) [Si$_2$O$_7$][SiO$_4$]$_3$O(OH)$_2$	^{A1}(Ca$_{0.93}$LREE$_{0.07}$)$^{A2-4}$LREE$_3$^{M1}(**Al$_{0.52}$**Fe^{3+}$_{0.34}$Mg$_{0.14}$) ^{M2}(**Al$_{1.88}$**Fe^{3+}$_{0.12}$)^{M3}(**Fe^{2+}**$_{0.53}$Mg$_{0.24}$Mn$_{0.16}$Fe^{3+}$_{0.07}$) [Si$_2$O$_7$][SiO$_4$]$_3$O(OH)$_2$
Formula weight	1102.53	1103.53
Crystal size (mm)	0.07 × 0.11 × 0.20	0.03 × 0.05 × 0.07
Temperature (K)	293(2)	293(2)
Crystal system, space group, Z	Monoclinic, P2$_1$/m, 2	Monoclinic, P2$_1$/m, 2
Unit-cell dimensions (Å/°)	a = 8.9458(2), b = 5.72971(13), c = 17.6192(3) β = 115.9497(19)	a = 8.9652(4), b = 5.7306(2), c = 17.6770(9) β = 116.053(6)
V, Å^3	812.06(3)	815.88(7)
Absorption coefficient μ, (mm^{-1})	10.41	10.37
F$_{000}$	1023	1024
Data collection		
Diffractometer	Xcalibur S CCD	Xcalibur S CCD
Radiation and wavelength (Å)	MoKα; 0.71073	MoKα; 0.71073
θ range for data collection (°)	2.71–30.51	3.30–28.28
Reflections collected	15,902	14,151
Independent reflections	2696 (R_{int} = 0.0398)	2218 (R_{int} = 0.0710)
Independent reflections with $I > 2σ(I)$	2532	2040
Data reduction	*CrysAlisPro*, Agilent Technologies, Version 1.171.37.35 (Agilent Technologies, 2014)	
Absorption correction	Gaussian	Gaussian
Index ranges	–12 ≤ h ≤ 12, –8 ≤ k ≤ 8, –25 ≤ l ≤ 25	–11 ≤ h ≤ 11, –7 ≤ k ≤ 7, –23 ≤ l ≤ 23
Refinement		
Structure solution/ Refinement method	direct methods/full–matrix least–squares on F^2	full–matrix least–squares on F^2
Number of refined parameters	202	199
Final R indices [$I > 2σ(I)$]	R_1 = 0.0355, wR_2* = 0.0679	R_1 = 0.0752, wR_2* = 0.1186
R indices (all data)	R_1 = 0.0401, wR_2* = 0.0695	R_1 = 0.0850, wR_2* = 0.1218
GoF	1.212	1.384
Largest diff. peak and hole, e^-/Å^3	2.21 and –2.28	2.35 and –2.14

*$w = 1/[σ^2(F_o^2) + (0.0186P)^2 + 5.3816P]$; $P = ([max of (0 or F_o^2)] + 2F_c^2)/3$ for ferriperbøeite-(La).
$w = 1/[σ^2(F_o^2) + (0.0240P)^2 + 16.4905P]$; $P = ([max of (0 or F_o^2)] + 2F_c^2)/3$ for perbøeite-(La).

Table 5. Coordinates, equivalent displacement parameters (U_{eq}, in Å^2) and anisotropic displacement parameters of atoms (excepting H) and site occupancy factors (s.o.f.) for ferriperbøeite-(La) and perbøeite-(La).

Site	x	y	z	U_{eq}	s.o.f.	U^{11}	U^{22}	U^{33}	U^{23}	U^{13}	U^{12}
Ferriperbøeite-(La)											
A(1)	0.72989(17)	¼	0.40886(8)	0.0148(4)	$Ca_{0.967(3)}LREE_{0.033(3)}$	0.0201(7)	0.0131(7)	0.0157(7)	0.000	0.0118(5)	0.000
A(2)	0.89196(5)	¼	0.25027(2)	0.01221(9)	$LREE_{1.00}$	0.00944(16)	0.01552(19)	0.00960(16)	0.000	0.00225(13)	0.000
A(3)	0.73868(6)	¼	0.00917(3)	0.02711(12)	$LREE_{1.00}$	0.0173(2)	0.0522(3)	0.00800(18)	0.000	0.00200(15)	0.000
A(4)	0.07678(5)	¾	0.16593(2)	0.01192(9)	$LREE_{1.00}$	0.00950(16)	0.01425(19)	0.01005(16)	0.000	0.00248(13)	0.000
M(1)	½	½	½	0.0097(3)	$Fe_{0.44}Al_{0.36}Mg_{0.20}$*	0.0078(5)	0.0079(6)	0.0120(6)	0.0005(5)	0.0030(5)	0.0009(5)
M(2)	0.47953(15)	0.0000(2)	0.20518(8)	0.0087(4)	$Al_{0.952(6)}Fe_{0.048(6)}$	0.0069(6)	0.0065(6)	0.0112(6)	−0.0001(4)	0.0025(5)	−0.0001(4)
M(3)	0.19082(13)	¾	0.37681(7)	0.0112(2)	$Fe_{0.63}Mg_{0.22}Mn_{0.15}$*	0.0086(5)	0.0103(5)	0.0094(5)	0.000	−0.0009(4)	0.000
Si(1)	0.1588(2)	¼	0.47874(10)	0.0069(3)	$Si_{1.00}$	0.0061(7)	0.0060(8)	0.0068(7)	0.000	0.0013(6)	0.000
Si(2)	0.8015(2)	¾	0.33460(11)	0.0071(3)	$Si_{1.00}$	0.0062(7)	0.0054(8)	0.0093(7)	0.000	0.0031(6)	0.000
Si(3)	0.3027(2)	¼	0.31192(10)	0.0066(3)	$Si_{1.00}$	0.0058(7)	0.0059(8)	0.0076(7)	0.000	0.0025(6)	0.000
Si(4)	0.6692(2)	¾	0.10312(11)	0.0093(3)	$Si_{1.00}$	0.0080(7)	0.0101(8)	0.0096(8)	0.000	0.0036(6)	0.000
Si(5)	0.1548(2)	¼	0.07854(11)	0.0073(3)	$Si_{1.00}$	0.0049(7)	0.0069(8)	0.0081(7)	0.000	0.0009(6)	0.000
O(1)	0.2623(4)	0.4899(6)	0.4828(2)	0.0135(7)	$O_{1.00}$	0.0122(15)	0.0088(16)	0.0188(16)	−0.0016(13)	0.0062(13)	−0.0019(13)
O(2)	0.1781(4)	0.4739(6)	0.2900(2)	0.0112(6)	$O_{1.00}$	0.0097(14)	0.0109(16)	0.0119(14)	0.0040(12)	0.0038(12)	0.0044(12)
O(3)	0.6911(4)	0.9861(6)	0.2991(2)	0.0116(6)	$O_{1.00}$	0.0094(14)	0.0070(15)	0.0143(15)	−0.0002(12)	0.0014(12)	0.0003(12)
O(4)	0.4389(6)	¾	0.4225(3)	0.0131(9)	$O_{1.00}$	0.010(2)	0.011(2)	0.015(2)	0.000	0.0019(18)	0.000
O(5)	0.4494(5)	¼	0.4111(3)	0.0112(9)	$O_{1.00}$	0.007(2)	0.013(2)	0.011(2)	0.000	0.0009(17)	0.000
O(6)	0.4145(6)	¼	0.2585(2)	0.0099(9)	$O_{1.00}$	0.010(2)	0.010(2)	0.011(2)	0.000	0.0056(17)	0.000
O(7)	−0.0173(6)	¼	0.3981(3)	0.0131(9)	$O_{1.00}$	0.010(2)	0.017(2)	0.009(2)	0.000	0.0014(17)	0.000
O(8)	0.9488(6)	¾	0.3066(3)	0.0217(12)	$O_{1.00}$	0.011(2)	0.038(3)	0.020(3)	0.000	0.011(2)	0.000
O(9)	0.8759(6)	¾	0.4374(3)	0.0198(11)	$O_{1.00}$	0.019(3)	0.030(3)	0.010(2)	0.000	0.007(2)	0.000
O(10)	0.5586(6)	¼	0.1633(3)	0.0105(9)	$O_{1.00}$	0.009(2)	0.016(2)	0.0047(19)	0.000	0.0014(16)	0.000
H(1)	0.512(9)	¼	0.1097(7)	0.013**	$H_{1.00}$						
O(11)	0.4006(5)	¾	0.2478(3)	0.0085(8)	$O_{1.00}$	0.0066(19)	0.009(2)	0.009(2)	0.000	0.0028(16)	0.000
H(2)	0.418(10)	¾	0.2993(16)	0.010**	$H_{1.00}$						
O(12)	0.5390(5)	¾	0.1478(3)	0.0106(9)	$O_{1.00}$	0.0054(19)	0.012(2)	0.016(2)	0.000	0.0053(17)	0.000
O(13)	0.2671(4)	0.4882(6)	0.1100(2)	0.0122(6)	$O_{1.00}$	0.0091(14)	0.0061(15)	0.0180(16)	−0.0008(12)	0.0029(12)	−0.0007(12)
O(14)	0.7926(4)	−0.0267(6)	0.1316(2)	0.0164(7)	$O_{1.00}$	0.0176(16)	0.0102(16)	0.0293(19)	0.0000(14)	0.0176(15)	0.0000(14)
O(15)	0.5521(8)	0.6817(12)	0.0046(4)	0.0158(15)	$O_{0.50}$	0.018(3)	0.017(4)	0.009(3)	−0.004(2)	0.003(2)	−0.003(2)
O(16)	0.0611(8)	¼	−0.0219(3)	0.0340(15)	$O_{1.00}$	0.038(4)	0.044(4)	0.007(2)	0.000	−0.002(2)	0.000
O(17)	0.0232(6)	¼	0.1176(3)	0.0217(12)	$O_{1.00}$	0.011(2)	0.037(3)	0.019(3)	0.000	0.008(2)	0.000
Perbøeite-(La)											
A(1)	0.7304(4)	¼	0.40892(19)	0.0197(11)	$Ca_{0.933(7)}LREE_{0.067(7)}$	0.0292(18)	0.0158(17)	0.0214(17)	0.000	0.0179(13)	0.000
A(2)	0.89180(11)	¼	0.25072(5)	0.0147(2)	$LREE_{1.00}$	0.0123(4)	0.0172(5)	0.0118(4)	0.000	0.0027(3)	0.000
A(3)	0.73836(13)	¼	0.00931(6)	0.0314(3)	$LREE_{1.00}$	0.0232(5)	0.0552(8)	0.0104(5)	0.000	0.0025(4)	0.000
A(4)	0.07783(11)	¾	0.16589(6)	0.0140(2)	$LREE_{1.00}$	0.0129(4)	0.0150(5)	0.0124(4)	0.000	0.0039(3)	0.000
M(1)	½	½	½	0.0111(7)	$Al_{0.52}Fe^{3+}_{0.34}Mg_{0.14}$*	0.0104(15)	0.0057(16)	0.0167(16)	−0.0004(12)	0.0054(13)	0.0011(12)
M(2)	0.4794(4)	0.0005(6)	0.20533(19)	0.0120(9)	$Al_{0.935(13)}Fe_{0.065(13)}$	0.0103(16)	0.0093(16)	0.0144(16)	0.0000(11)	0.0036(12)	0.0006(11)
M(3)	0.1888(5)	¾	0.37674(16)	0.0149(6)	$Fe_{0.60}Mg_{0.24}Mn_{0.16}$*	0.0127(12)	0.0115(13)	0.0112(12)	0.000	−0.0034(10)	0.000
Si(1)	0.1595(5)	¼	0.4790(2)	0.0079(8)	$Si_{1.00}$	0.0077(18)	0.0055(19)	0.0075(18)	0.000	0.0006(15)	0.000
Si(2)	0.8003(5)	¾	0.3351(3)	0.0094(8)	$Si_{1.00}$	0.0089(19)	0.006(2)	0.013(2)	0.000	0.0042(16)	0.000
Si(3)	0.3025(5)	¼	0.3118(2)	0.0085(8)	$Si_{1.00}$	0.0095(19)	0.007(2)	0.0094(19)	0.000	0.0046(15)	0.000
Si(4)	0.6700(5)	¾	0.1037(3)	0.0126(8)	$Si_{1.00}$	0.013(2)	0.012(2)	0.014(2)	0.000	0.0062(17)	0.000
Si(5)	0.1550(5)	¼	0.0782(3)	0.0091(8)	$Si_{1.00}$	0.0062(18)	0.008(2)	0.0124(19)	0.000	0.0034(15)	0.000
O(1)	0.2624(9)	0.4909(13)	0.4834(5)	0.0170(17)	$O_{1.00}$	0.018(4)	0.003(4)	0.032(4)	−0.005(3)	0.013(3)	−0.003(3)
O(2)	0.1784(9)	0.4742(14)	0.2901(5)	0.0153(16)	$O_{1.00}$	0.013(4)	0.016(4)	0.017(4)	0.006(3)	0.006(3)	0.007(3)
O(3)	0.6912(9)	0.9866(13)	0.2998(5)	0.0145(16)	$O_{1.00}$	0.015(4)	0.004(4)	0.020(4)	−0.001(3)	0.004(3)	0.002(3)
O(4)	0.4382(13)	¾	0.4239(7)	0.017(2)	$O_{1.00}$	0.015(5)	0.011(6)	0.021(6)	0.000	0.005(5)	0.000
O(5)	0.4485(12)	¼	0.4109(6)	0.015(2)	$O_{1.00}$	0.007(5)	0.017(6)	0.012(5)	0.000	−0.003(4)	0.000
O(6)	0.4142(12)	¼	0.2586(6)	0.012(2)	$O_{1.00}$	0.008(5)	0.016(6)	0.014(5)	0.000	0.006(4)	0.000
O(7)	−0.0161(12)	¼	0.3978(6)	0.014(2)	$O_{1.00}$	0.008(5)	0.019(6)	0.012(5)	0.000	0.002(4)	0.000
O(8)	0.9490(14)	¾	0.3069(8)	0.025(3)	$O_{1.00}$	0.014(6)	0.043(8)	0.025(6)	0.000	0.015(5)	0.000
O(9)	0.8755(15)	¾	0.4371(7)	0.025(3)	$O_{1.00}$	0.028(7)	0.037(8)	0.008(5)	0.000	0.006(5)	0.000
O(10)	0.5577(13)	¼	0.1639(7)	0.014(2)**	$O_{1.00}$						
H(1)	0.512(19)	¼	0.1103(9)	0.016**	$H_{1.00}$						
O(11)	0.4007(12)	¾	0.2471(6)	0.009(2)	$O_{1.00}$	0.011(5)	0.012(5)	0.005(5)	0.000	0.004(4)	0.000
H(2)	0.415(19)	¾	0.298(3)	0.011**	$H_{1.00}$						
O(12)	0.5388(11)	¾	0.1480(6)	0.010(2)	$O_{1.00}$	0.003(4)	0.005(5)	0.019(5)	0.000	0.002(4)	0.000
O(13)	0.2680(9)	0.4876(13)	0.1095(5)	0.0150(16)	$O_{1.00}$	0.014(4)	0.005(4)	0.021(4)	−0.002(3)	0.002(3)	0.000(3)
O(14)	0.7930(10)	−0.0272(14)	0.1321(5)	0.0191(17)	$O_{1.00}$	0.023(4)	0.012(4)	0.034(5)	0.003(3)	0.023(4)	0.001(3)
O(15)	0.5525(19)	0.684(3)	0.0055(9)	0.023(4)	$O_{0.50}$	0.037(9)	0.020(12)	0.008(6)	0.002(5)	0.006(4)	−0.005(7)
O(16)	0.0628(18)	¼	−0.0218(8)	0.040(4)	$O_{1.00}$	0.044(8)	0.055(10)	0.007(6)	0.000	−0.001(6)	0.000
O(17)	0.0241(14)	¼	0.1161(8)	0.028(3)	$O_{1.00}$	0.011(6)	0.042(9)	0.029(7)	0.000	0.007(5)	0.000

*Fixed during the refinement.

For ferriperbøeite-(La): M(1) Al *vs.* Fe was refined (e_{ref} 18.46), for M(3) Fe *vs.* Mg was refined (e_{ref} 22.78). Thus, based on chemical data, cation-anion distances, charge-balance requirements and e_{ref}, M(1) site was assumed to be occupied by ($Fe^{3+}_{0.44}Al_{0.36}Mg_{0.20}$) possibly with minor Ti admixture; M(3) octahedron – by ($Fe^{2+}_{0.46}Mg_{0.22}Fe^{3+}_{0.17}Mn_{0.15}$).

For perbøeite-(La): M(1) Al *vs.* Fe was refined (e_{ref} 17.24), for M(3) Fe *vs.* Mg was refined (e_{ref} 22.47). Thus, based on chemical data, cation-anion distances, charge-balance requirements and e_{ref}, the M(1) site was assumed to be occupied by ($Al_{0.52}Fe^{3+}_{0.34}Mg_{0.14}$), possibly with minor Ti admixture, and M(3) by ($Fe^{2+}_{0.53}Mg_{0.24}Mn_{0.16}Fe^{3+}_{0.07}$).

**U_{iso}.

Table 6. Selected interatomic distances (Å) and angles (°) in the structure of ferriperbøeite-(La) and perbøeite-(La).

Ferriperbøeite-(La)				Perbøeite-(La)			
A(1)–O(7)	2.351(5)	M(2)–O(10)	1.885(3)	A(1)–O(3)	2.350(8) x2	M(2)–O(10)	1.878(8)
A(1)––O(3)	2.358(3) x2	M(2)–O(11)	1.892(3)	A(1)–O(7)	2.365(11)	M(2)–O(11)	1.888(7)
A(1)––O(1)	2.398(4) x2	M(2)–O(3)	1.894(3)	A(1)–O(1)	2.393(8) x2	M(2)–O(3)	1.902(8)
A(1)––O(5)	2.527(5)	M(2)–O(13)	1.907(3)	A(1)–O(5)	2.543(11)	M(2)–O(13)	1.909(8)
A(1)––O(6)	2.905(5)	M(2)–O(6)	1.937(3)	A(1)–O(6)	2.913(10)	M(2)–O(6)	1.938(8)
A(1)––O(9)	3.097(2) x2	M(2)–O(12)	1.957(3)	A(1)–O(9)	3.095(5) x2	M(2)–O(12)	1.961(8)
<A(1)–O>	2.610	<M(2)–O>	1.912	<A(1)–O>	2.61	<M(2)–O>	1.913
A(2)–O(7)	2.365(5)	M(3)–O(8)	1.968(5)	A(2)–O(7)	2.357(10)	M(3)–O(8)	1.953(12)
A(2)–O(14)	2.460(4) x2	M(3)–O(4)	2.002(5)	A(2)–O(14)	2.465(8) x2	M(3)–O(4)	2.014(11)
A(2)–O(2)	2.668(3) x2	M(3)–O(2)	2.169(3) x2	A(2)–O(2)	2.677(8) x2	M(3)–O(2)	2.174(8) x2
A(2)–O(10)	2.691(4)	M(3)–O(1)	2.253(4) x2	A(2)–O(10)	2.700(10)	M(3)–O(1)	2.258(8) x2
A(2)–O(3)	2.758(3) x2	<M(3)–O>	2.136	A(2)–O(3)	2.763(8) x2	<M(3)–O>	2.14
A(2)–O(8)	3.0017(16) x2			A(2)–O(8)	3.002(4) x2		
A(2)–O(17)	3.041(5)	Si(1)–O(7)	1.595(5)	A(2)–O(17)	3.090(13)	Si(1)–O(7)	1.598(11)
<A(2)–O>	2.716	Si(1)–O(9)	1.638(5)	<A(2)–O>	2.72	Si(1)–O(1)	1.644(8) x2
		Si(1)–O(1)	1.641(3) x2			Si(1)–O(9)	1.644(12)
A(3)–O(17)	2.423(5)	<Si(1)–O>	1.629	A(3)–O(17)	2.425(11)	<Si(1)–O>	1.63
A(3)–O(15)	2.535(7)			A(3)–O(15)	2.532(16)		
A(3)–O(14)	2.547(4) x2	Si(2)–O(8)	1.596(5)	A(3)–O(14)	2.557(8) x2	Si(2)–O(8)	1.615(12)
A(3)–O(13)	2.563(3) x2	Si(2)–O(3)	1.630(3) x2	A(3)–O(13)	2.563(8) x2	Si(2)–O(9)	1.624(11)
A(3)–O(12)	2.794(5)	Si(2)–O(9)	1.633(5)	A(3)–O(12)	2.800(10)	Si(2)–O(3)	1.627(8) x2
A(3)–O(15)	2.965(7)	<Si(2)–O>	1.622	A(3)–O(15)	2.977(16)	<Si(2)–O>	1.62
A(3)–O(16)	3.162(7)			A(3)–O(16)	3.188(15)		
A(3)–O(16)	3.334(4) x2	Si(3)–O(2)	1.631(3) x2	A(3)–O(16)	3.331(8) x2	Si(3)–O(2)	1.631(8) x2
<A(3)–O>	2.797	Si(3)–O(6)	1.646(5)	<A(3)–O>	2.82	Si(3)–O(6)	1.648(11)
		Si(3)–O(5)	1.663(5)			Si(3)–O(5)	1.663(11)
A(4)–O(16)	2.285(5)	<Si(3)–O>	1.643	A(4)–O(16)	2.293(12)	<Si(3)–O>	1.64
A(4)–O(2)	2.524(3) x2			A(4)–O(2)	2.528(7) x2		
A(4)–O(11)	2.611(4)	Si(4)–O(14)	1.619(4) x2	A(4)–O(11)	2.605(10)	Si(4)–O(14)	1.617(8) x2
A(4)–O(14)	2.669(3) x2	Si(4)–O(15)	1.635(6)	A(4)–O(14)	2.677(8) x2	Si(4)–O(15)	1.632(15)
A(4)–O(13)	2.754(3) x2	Si(4)–O(12)	1.667(5)	A(4)–O(13)	2.767(8) x2	Si(4)–O(12)	1.674(11)
A(4)–O(17)	2.9675(14) x2	<Si(4)–O>	1.635	A(4)–O(17)	2.974(3) x2	<Si(4)–O>	1.64
A(4)–O(8)	3.153(5)			A(4)–O(8)	3.174(11)		
<A(4)–O>	2.716	Si(5)–O(16)	1.592(5)	<A(4)–O>	2.72	Si(5)–O(17)	1.587(13)
		Si(5)–O(17)	1.602(5)			Si(5)–O(16)	1.588(12)
M(1)–O(4)	1.887(3) x2	Si(5)–O(13)	1.641(3) x2	M(1)–O(4)	1.875(7) x2	Si(5)–O(13)	1.642(8) x2
M(1)–O(1)	2.014(3) x2	<Si(5)–O>	1.619	M(1)–O(1)	2.019(7) x2	<Si(5)–O>	1.61
M(1)–O(5)	2.023(3) x2			M(1)–O(5)	2.027(7) x2		
<M(1)–O>	1.975			<M(1)–O>	1.974		

360–630 cm^{-1}, to mixed modes and overlapping bands of Al–O and Fe^{3+}–O stretching vibrations, as well as bending vibrations of silicate groups.

Unlike allanite-group minerals, where the strongest band of Si–O-stretching vibrations in IR spectra is observed between 915 and 940 cm^{-1} and belongs to the Si$_2$O$_7$ groups (Chukanov, 2014; Chukanov and Chervonnyi, 2016), the main IR absorption band of ferriperbøeite-(La) has a maximum at 870 cm^{-1} which corresponds to vibrations of SiO$_4$ groups.

Chemical composition

Chemical data for both new minerals were obtained using a Cameca SX-100 electron microprobe (wavelength-dispersive spectroscopy mode, acceleration voltage of 15 kV, a beam current of 20 nA, and a 3 μm beam diameter). The spectral interference of F$K\alpha$ and Ce$M\zeta$ were corrected manually using empirically determined correction factors. H$_2$O was not determined directly due to the scarcity of pure material and was calculated by stoichiometry on the basis of O$_{20}$(OH,F)$_2$ taking into account that bond-valence sums for the sites O(10) and O(11) are close to 1.0 (see below). Both crystal structure and Raman spectroscopy data confirm the presence of OH groups and the absence of carbonate and borate groups in both new species.

Despite the fact that ferriperbøeite-(La) and perbøeite-(La) are 'common' at the deposit, attempts to determine the valence state of iron using Mössbauer spectroscopy were unsuccessful due to lack of pure material: small but abundant inclusions of allanite/

Table 7. Hydrogen-bond lengths (*d* in Å) and angles (in °) for ferriperbøeite-(La) and perbøeite-(La).

Ferriperbøeite-(La)					Perbøeite-(La)				
D–H⋯*A*	*D*–H	H⋯*A*	*D*⋯*A*	∠(*D*–H⋯*A*)	*D*–H⋯*A*	*D*–H	H⋯*A*	*D*⋯*A*	∠(*D*–H⋯*A*)
O(10)–H(1)⋯O(15)	0.850(10)	1.878(18)	2.706(8)	165(5)	O(10)–H(1)⋯O(15)	0.850(10)	1.91(3)	2.735(18)	165(10)
O(10)–H(1)⋯O(15)	0.850(10)	1.878(18)	2.706(8)	165(5)	O(10)–H(1)⋯O(15)	0.850(10)	1.91(3)	2.735(18)	165(10)
O(11)–H(2)⋯O(4)	0.851(10)	2.096(14)	2.944(7)	175(8)	O(11)–H(2)⋯O(4)	0.851(10)	2.14(2)	2.992(15)	177(15)

D – donor; *A* – acceptor.
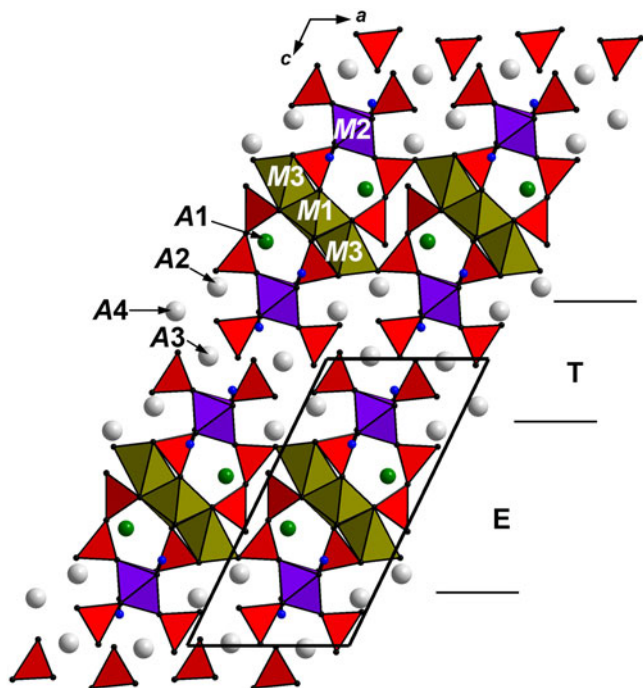
Fig. 11. The crystal structure of ferriperbøeite-(La)/perbøeite-(La). SiO$_4$ tetrahedra are red. H atoms of OH groups are shown as small blue circles. Alternation of (001) epidote-type slabs (**E**) and ($\bar{1}$02) törnebohmite-type slabs (**T**) is shown. The unit cell is outlined.

ferriallanite in both new minerals significantly affected the reproducibility of the data. For this reason, the Fe^{3+}:Fe^{2+} ratio reported herein is based on the bond-valence calculations and charge-balance requirements.

Chemical data are presented in Table 3, any other element with atomic numbers higher than that of carbon, not listed in Table 3, were below detection limits.

The empirical formulae calculated on the basis of O$_{20}$(OH,F)$_2$ are: ferriperbøeite-(La), (Ca$_{0.95}$La$_{1.58}$Ce$_{1.30}$Nd$_{0.10}$Pr$_{0.06}$)$_{\Sigma3.99}$(Al$_{2.27}$Fe$^{3+}_{0.72}$Fe$^{2+}_{0.46}$Mg$_{0.40}$Mn$_{0.16}$Ti$_{0.03}$)$_{\Sigma4.04}$Si$_{4.96}$O$_{20}$[(OH)$_{1.94}$F$_{0.06}$] and perbøeite-(La), (Ca$_{0.94}$Th$_{0.01}$La$_{1.49}$Ce$_{1.34}$Nd$_{0.14}$Pr$_{0.07}$)$_{\Sigma3.99}$(Al$_{2.42}$Fe$^{3+}_{0.52}$Fe$^{2+}_{0.51}$Mg$_{0.38}$Mn$_{0.14}$Ti$_{0.03}$)$_{\Sigma4.00}$Si$_{4.99}$O$_{20}$[(OH)$_{1.87}$F$_{0.13}$].

The idealised formulae are as follows. Ferriperbøeite-(La): (CaLa$_3$)(Fe^{3+}Al$_2$Fe^{2+})[Si$_2$O$_7$][SiO$_4$]$_3$O(OH)$_2$ which requires CaO 5.03, FeO 6.43, La$_2$O$_3$ 43.76, Fe$_2$O$_3$ 7.15, Al$_2$O$_3$ 9.14, SiO$_2$ 26.88, H$_2$O 1.61, total 100 wt.%. Perbøeite-(La): (CaLa$_3$)(Al$_3$Fe^{2+})[Si$_2$O$_7$][SiO$_4$]$_3$O(OH)$_2$ which requires CaO 5.14, FeO 6.58, La$_2$O$_3$ 44.93, Al$_2$O$_3$ 14.07, SiO$_2$ 27.62, H$_2$O 1.66, total 100 wt.%.

X-ray crystallography

Powder XRD data for both minerals were collected with a Rigaku R-AXIS Rapid II single-crystal diffractometer equipped with cylindrical image plate detector (radius 127.4 mm) using Debye-Scherrer geometry, Co*K*α radiation (rotating anode with VariMAX microfocus optics), 40 kV, 15 mA and an exposure of 15 min. Angular resolution of the detector is 0.045°2θ (pixel size 0.1 mm). The data were integrated using the software package *osc2tab* (Britvin *et al.*, 2017). The powder XRD data for both minerals are given in Supplementary material (Table S2 and Table S3, see below). Both minerals are monoclinic, with unit-cell parameters calculated from the powder data, $a = 8.951(5)$, $b =$

5.737(2), $c = 17.65(1)$ Å, $\beta = 115.97(4)°$ and $V = 815(1)$ Å^3 for ferriperbøeite-(La) and $a = 8.964(8)$, $b = 5.738(2)$, $c = 17.69(2)$ Å, $\beta = 116.04(5)°$ and $V = 817(1)$ Å^3 for perbøeite-(La).

Single-crystal X-ray studies of both new minerals were carried out using an Xcalibur S diffractometer equipped with a CCD detector. A full sphere of three-dimensional data was collected. Data reduction was performed using *CrysAlisPro* Version 1.171.37.35 (Agilent Technologies, 2014). The data were corrected for Lorentz factor and polarisation effect.

The crystal structure of ferriperbøeite-(La) was solved by direct methods and refined with the use of the *SHELX-97* software package (Sheldrick, 2008) to $R = 0.0355$ for 2532 unique reflections with $I > 2\sigma(I)$. The crystal structure of perbøeite-(La) was refined to $R = 0.0752$ for 2040 unique reflections with $I > 2\sigma(I)$ on the basis of atomic coordinates of ferriperbøeite-(La). The H atoms of the OH groups of both minerals were located from the difference-Fourier synthesis and their positions were restricted to keep O–H distances of 0.85(1) Å and U_{iso} (H) = 1.2 U_{eq} (O).

The crystal dimensions, data collection information and structure refinement details for ferriperbøeite-(La) and perbøeite-(La) are given in Table 4, atomic coordinates, thermal displacement parameters of atoms and site occupancies in Table 5 and selected interatomic distances in Table 6. Hydrogen bond lengths are in Table 7 and bond-valence calculations are given in Supplementary material (Table S4).

The crystallographic information files for both minerals have been deposited with the Principal Editor of *Mineralogical Magazine* and are available as Supplementary material (see below).

Crystal structure

Ferriperbøeite-(La) and perbøeite-(La) are isostructural (Fig. 11). They are two new members of the recently IMA-approved gatelite supergroup (Bonazzi *et al.*, 2019) which includes minerals with the general formula A_4M_4(Si$_2$O$_7$)(SiO$_4$)$_3$(O,F)(OH)$_2$. The A sites are occupied by cations in large cavities: Ca (*A*1) and *REE* +/– Na (*A*2, *A*3 and *A*4). The M sites are octahedrally coordinated and occupied by di- and trivalent cations, i.e. Al, Fe^{2+}, Fe^{3+}, Mg, Mn^{2+} and Mn^{3+}. Lower in the hierarchy, the gatelite supergroup is divided into three mineral groups. Ferriperbøeite-(La) and perbøeite-(La) should be included into the gatelite group along with gatelite-(Ce) (CaCe$_3$)(Al$_3$Mg)[Si$_2$O$_7$][SiO$_4$]$_3$O(OH)$_2$ (Bonazzi *et al.*, 2003), perbøeite-(Ce) (CaCe$_3$)(Al$_3$Fe^{2+})[Si$_2$O$_7$] (SiO$_4$)$_3$O(OH)$_2$ (Bonazzi *et al.*, 2014) and ferriperbøeite-(Ce) (CaCe$_3$)(Fe^{3+} Al$_2$Fe^{2+})[Si$_2$O$_7$][SiO$_4$]$_3$O(OH)$_2$ (Bindi *et al.*, 2018). This group includes members with formulae that can be derived from gatelite-(Ce) solely by homovalent substitutions. The key cation and anion sites for this group are: *A*1 = A^{2+}; *A*2, *A*3 and *A*4 = A^{3+}; *M*1 = M^{3+}; *M*2 = M^{3+}; *M*3 = M^{2+}; O4 = O^{2-}; O10 and O11 = (OH)$^-$ (Bonazzi *et al.*, 2019). Thus, the species-defining cations for ferriperbøeite-(La) are Ca (*A*1), La (*A*2–4), Fe^{3+} (*M*1), Al (*M*2), and Fe^{2+} (*M*3); for perbøeite-(La) these are Ca (*A*1), La (*A*2–4), Al (*M*1), Al (*M*2) and Fe^{2+} (*M*3) [Table 4]. For comparison of all five members of the gatelite group see Table 8.

All the minerals of the gatelite supergroup are considered as iso-topological **ET** type polysomes within a polysomatic series which has epidote-type (**E**) and törnebohmite-type (**T**) structures as end-members. Their structure can be described as a regular alternating 1:1 stacking of slabs of (**E**) and (**T**) structures (Bonazzi *et al.*, 2014, 2019). The **E** modules are (001) slabs with the general composition $A_2M1M2M3$[Si$_2$O$_7$][SiO$_4$]X(OH), where X = O^{2-} and/or F$^-$ and the **T** modules are ($\bar{1}$02) slabs with the

Table 8. Comparative data for the members of the gatelite group.

Mineral	Ferriperbøeite-(La)	Perbøeite-(La)	Perbøeite-(Ce)	Ferriperbøeite-(Ce)	Gatelite-(Ce)
End-member formula	$(CaLa_3)(Fe^{3+}Al_2Fe^{2+})$ $[Si_2O_7]$ $[SiO_4]_3O(OH)_2$	$(CaLa_3)(Al_3Fe^{2+})$ $[Si_2O_7]$ $[SiO_4]_3O(OH)_2$	$(CaCe_3)(Al_3Fe^{2+})$ $[Si_2O_7]$ $[SiO_4]_3O(OH)_2$	$(CaCe_3)(Fe^{3+}Al_2Fe^{2+})$ $[Si_2O_7]$ $[SiO_4]_3O(OH)_2$	$(CaCe_3)(Al_3Mg)$ $[Si_2O_7]$ $[SiO_4]_3O(OH)_2$
E module composition	Ferriallanite-(La)	Allanite-(La)	Allanite-(Ce)	Ferriallanite-(Ce)	Dissakisite-(Ce)
T module composition	Törnebohmite-(La)	Törnebohmite-(La)	Törnebohmite-(Ce)	Törnebohmite-(Ce)	Törnebohmite-(Ce)
Crystal system	Monoclinic	Monoclinic	Monoclinic	Monoclinic	Monoclinic
Space group	$P2_1/m$	$P2_1/m$	$P2_1/m$	$P2_1/m$	$P2_1/a$
a (Å)	8.9458(2)	8.9652(4)	8.9277(6)	8.9320(4)	17.770(4)
b (Å)	5.72971(13)	5.7306(2)	5.6548(6)	5.7280(3)	5.651(1)
c (Å)	17.6192(3)	17.6770(9)	17.587(1)	17.5549(9)	17.458(4)
$β$ (°)	115.9497(19)	116.053(6)	116.475(8)	116.030(4)	116.18(2)
V (Å^3)	812.06(3)	815.88(6)	794.8(1)	807.05(7)	1573.3(6)
Z	2	2	2	2	4
Strongest lines of the powder X-ray diffraction pattern: d (Å) – I (%)	15.81–72 4.70–43 3.521–53 3.003–100 2.636–60	15.85–83 4.665–68 3.523–99 3.116–56 3.009–100	15.71–91 3.501–44 2.981–100 2.843–48 2.619–59	3.520–45 2.997–100 2.868–45 2.771–40 2.633–60	15.67–87 3.49–50 2.97–100 2.83–44 2.61–56
Colour	Brownish black	Brownish black	Greyish green	Brownish black	Colourless
Density (calc.) (g cm^{-3})	4.510	4.483	4.474	4.634	4.51
Optical data:					
Optical sign	Biaxial (+)	Biaxial (+)	Biaxial (+)	Biaxial (+)	
$α$	1.788(5)	1.778(8)	1.788(2)	No data	
$β$	1.790(5)	1.783(8)	1.793(2)	No data	
$γ$	1.810(5)	1.805(8)	1.820(5)	No data	No data
2V, (°)	40(10)	40(10)	30(5)	65(5)	
Pleochroism	Weak, from nearly colourless and pale-brownish to greenish-brown	Strong, from colourless and brownish to dirty-brown	Very weak, from colourless to greyish blue	Strong from green, throughout orange-brown, to deep red	
Source	This paper	This paper	Bonazzi *et al.* (2014)	Bindi *et al.* (2018)	Bonazzi *et al.* (2003)

composition [$REE_2Al(SiO_4)_2(OH)$] (Fig. 11). In ferriperbøeite-(La) and perbøeite-(La), the **T** module is the same and corresponds to a törnebohmite-(La) composition, but the **E** module is different and has a ferriallanite-(La) composition in ferriperbøeite-(La) and an allanite-(La) composition in perbøeite-(La).

The crystal structure of ferriperbøeite-(La) and perbøeite-(La) consists of chains of edge-sharing octahedra running along the *b* axis: single chains of the *M*(2)-centred octahedra and branched chains with the *M*(1)-centred octahedra in the central part and the *M*(3)-centred octahedra attached to them from both sides. The chains are linked *via* isolated [SiO_4] tetrahedra and disilicate groups [Si_2O_7]. The *A*(1–4) sites occur in large cavities. The angle Si(1)–O(9)–Si(2) in the disilicate group for both species is similar [148.7(4)° in ferriperbøeite-(La) and 148.3(8)° in perbøeite-(La)] and lies between the values reported for allanite- and epidote-group minerals: e.g. in ferriallanite-(La) this angle is equal to 143.61(12)° (Kolitsch *et al.*, 2012) and in epidote to 154.59(9)° (Gatta *et al.*, 2010).

The cation distribution (see below) was determined on the basis of chemical data, cation–anion distances, charge-balance requirements and the refined number of electrons (e_{ref}) values.

Despite La^{3+} being the dominant *REE* in ferriperbøeite-(La) and perbøeite-(La), the Ce scattering curve was used during the structure refinement of both minerals because of the significant content of Ce and only minor amounts of heavier Nd, Pr and, in the case of perbøeite-(La), very minor Th. According to refinement of the site occupation factors, the *A*(2–4) sites are occupied by *LREE* cations and the *A*(1) site is Ca-dominant with only a

minor *REE* admixture: the refined site populations are Ca$_{0.967(3)}$ *LREE*$_{0.033(3)}$ in ferriperbøeite-(La) and Ca$_{0.934(7)}$*LREE*$_{0.066(7)}$ in perbøeite-(La) Thus, the total composition of the *A* sites is [*LREE*$_{3.03}$Ca$_{0.97}$] in ferriperbøeite-(La) and [*LREE*$_{3.07}$Ca$_{0.93}$] in perbøeite-(La), which is in a good agreement with electron microprobe data (Table 3).

There are three octahedrally coordinated *M* sites, *M*(1–3). For the *M*(1) and *M*(2) sites, Al *vs.* Fe was refined, and for the *M*(3) site, Fe *vs.* Mg was refined. The *M*(2) site is Al-dominant in both new species with the refined population Al$_{0.953(6)}$Fe$_{0.047(6)}$ in ferriperbøeite-(La) and Al$_{0.936(13)}$Fe$_{0.064(13)}$ in perbøeite-(La). This site centres the smallest octahedron with the mean *M*(2)–O distance in ferriperbøeite-(La)/perbøeite-(La) being 1.912/1.913 Å, respectively.

The *M*(1)-centred octahedron is larger, with the mean *M*(1)–O distance in ferriperbøeite-(La)/perbøeite-(La) of 1.975/1.973 Å. The e_{ref} in the *M*(1) site is 18.46 in ferriperbøeite-(La) and only 17.24 in perbøeite-(La). This is the main difference between the two minerals. In ferriperbøeite-(La) this site is determined to be occupied predominantly by Fe^{3+} with subordinate Al and Mg cations in the atomic ratio Fe^{3+}:Al:Mg = 0.44:0.36:0.20, while in perbøeite-(La) it is determined to be occupied predominantly by Al with subordinate Fe^{3+} and Mg cations in the atomic ratio Al:Fe^{3+}:Mg = 0.52:0.34:0.14. A very minor Ti admixture is also determined to occur at the *M*(1) site of both minerals.

The largest *M*(3) octahedron with the mean *M*(3)–O distance of 2.136/2.14 Å in ferriperbøeite-(La)/perbøeite-(La), respectively,

is predominately occupied by Fe^{2+} with subordinate Mg, Mn and Fe^{3+}. According to electron microprobe data and refined numbers of electrons [e_{ref} = 22.78 in ferriperbøeite-(La) and 22.47 in perbøeite-(La)], we fixed the ratio Fe^{2+}:Mg:Fe^{3+}:Mn = 0.46:0.22:0.17:0.15 in ferriperbøeite-(La) and Fe^{2+}:Mg:Mn:Fe^{3+} = 0.53:0.24:0.16:0.07 in perbøeite-(La).

During the refinement, disorder was found for the O(15) site which deviates from the *m* plane just as it does in other members of the gatelite supergroup (see below). Bond-valence calculations (Table S4) confirm the above conclusions regarding cation distribution across different sites.

References

Agilent Technologies (2014) *CrysAlisPro Software system, version 1.171.37.34.* Agilent Technologies UK Ltd, Oxford, UK.

Alimarin I.P. (1930) On the chemical analysis of bastnäsite. Pp. 47–57 in: *Rare-Earth Minerals of Kyshtym Area. Trudy Instituta prikladnoy mineralogii* (*Proceedings of the Institute of Applied Mineralogy*), **44** [in Russian].

Alimova A.N., Pekov I.V., Kononkova N.N. and Kanonerov A.A. (2003) Ratios of lanthanoids in the rare-earth minerals of Mochalin Log, Southern Urals. *Materialy IV Vserossiyskogo soveshchaniya "Mineralogiya Urala – 2003"* (*Materials of IV*[th] *All-Russian Meeting "Mineralogy of Urals – 2003"*), Vol. 2, Miass, 158–162 [in Russian].

Allaz J., Raschke M. B., Persson P. M. and Stern C. R. (2015) Age, petrochemistry, and origin of a REE-rich mineralization in the Longs Peak-St. Vrain batholith, near Jamestown, Colorado (USA). *American Mineralogist*, **100**, 2123–2140.

Andò S. and Garzanti E. (2014) Raman spectroscopy in heavy-mineral studies. *Geological Society of London, Special Publications*, **386**, 395–412.

Bindi L., Holtstam D., Fantappiè G., Andersson U.B. and Bonazzi P. (2018) Ferriperbøeite-(Ce), $[CaCe_3]_{\Sigma=4}[Fe^{3+}Al_2Fe^{2+}]_{\Sigma=4}[Si_2O_7][SiO_4]_3O(OH)_2$, a new member of the polysomatic epidote–törnebohmite series from the Nya Bastnäs Fe–Cu–REE deposit, Sweden. *European Journal of Mineralogy*, **30**, 537–544.

Bonazzi P., Bindi L. and Parodi G. (2003) Gatelite-(Ce), a new *REE*-bearing mineral from Trimouns, French Pyrenees: crystal structure and polysomatic relationships with epidote and törnebohmite. *American Mineralogist*, **88**, 223–228.

Bonazzi P., Lepore G.O., Bindi L., Chopin C., Husdal T. and Medenbach O. (2014) Perbøeite-(Ce) and alnaperbøeite-(Ce), two new members of the epidote-törnebohmite polysomatic series: Chemistry, structure, dehydrogenation, and clue for a sodian epidote end-member. *American Mineralogist*, **99**, 157–169.

Bonazzi P., Holtstam D. and Bindi L. (2019) Gatelite-supergroup minerals: recommended nomenclature and review. *European Journal of Mineralogy*, **31**, 173–181.

Britvin S.N., Dolivo-Dobrovolsky D.V. and Krzhizhanovskaya M.G. (2017) Software for processing the X-ray powder diffraction data obtained from the curved image plate detector of Rigaku RAXIS Rapid II diffractometer. *Zapiski Rossiiskogo Mineralogicheskogo Obshchestva*, **146**, 104–107 [in Russian].

Chukanov N.V. (2014) *Infrared Spectra of Mineral Species: Extended Library.* Springer-Verlag, Dordrecht, 1716 pp.

Chukanov N.V. and Chervonnyi A.D. (2016) *Infrared Spectroscopy of Minerals and Related Compounds.* Springer-Verlag, Cham, 2016. 1109 pp.

Čopjaková R., Škoda R., Vašinová Galiová M., Novák M. and Cempírek J. (2015) Sc- and *REE*-rich tourmaline replaced by Sc-rich *REE*-bearing epidote-group mineral from the mixed (NYF plus LCT) Kracovice pegmatite (Moldanubian Zone, Czech Republic). *American Mineralogist*, **100**, 1434–1451.

Gatta G.D., Meven M. and Bromiley G. (2010) Effects of temperature on the crystal structure of epidote: a neutron single-crystal diffraction study at 293 and 1,070 K. *Physics and Chemistry of Minerals*, **37**, 475–485.

Holtstam D. and Andersson U.B. (2007) The *REE* minerals of the Bastnäs-type deposits, South-Central Sweden. *The Canadian Mineralogist*, **45**, 1073–1114.

Holtstam D., Kolitsch U. and Andersson U.B. (2005) Västmanlandite-(Ce) – a new lanthanide- and F-bearing sorosilicate mineral from Västmanland, Sweden: description, crystal structure, and relation to gatelite-(Ce). *European Journal of Mineralogy*, **17**, 129–141.

Kasatkin A.V., Pekov I.V., Zubkova N.V., Chukanov N.V., Škoda R., Polekhovsky Y.S., Belakovskiy D.I., Agakhanov A.A., Kuznetsov A.M. and Pushcharovsky D.Y. (2018) Ferriperbøeite-(La), IMA 2018-106. CNMNC Newsletter No. 46, December 2018, page 1377; *Mineralogical Magazine*, **82**, 1369–1379.

Kasatkin A.V., Pekov I.V., Zubkova N.V., Chukanov N.V., Škoda R., Polekhovsky Y.S., Belakovskiy D.I., Agakhanov A.A., Kuznetsov A.M. and Pushcharovsky D.Y. (2019) Perbøeite-(La), IMA 2018-116. CNMNC Newsletter No. 47, February 2019, page 144; *Mineralogical Magazine*, **83**, 143–147.

Knipovitch J.N. (1930) On the chemical composition of lessingite and cerite from Kystym district. Pp. 43–46 in: *Rare-Earth Minerals of Kyshtym Area. Trudy Instituta prikladnoy mineralogii* (*Proceedings of the Institute of Applied Mineralogy*), **44** [in Russian].

Kolitsch U., Mills S.J., Miyawaki R. and Blass G. (2012) Ferriallanite-(La), a new member of the epidote supergroup from the Eifel, Germany. *European Journal of Mineralogy*, **24**, 741–747.

Korovaev F. (1861) Kyshtymoparisite, a new mineral. *Gornyi Zhurnal (Mining Journal)*, **4**, 445–454 [in Russian].

Kuznetsov E.A. (1930) Petrographic review of Mochalin Log. Pp. 58–72 in: Rare-Earth Minerals of Kyshtym Area. Trudy Instituta Prikladnoy Mineralogii (Proceedings of the Institute of Applied Mineralogy), **44** [in Russian].

Levinson A.A. (1966) A system of nomenclature for rare-earth minerals. *American Mineralogist*, **51**, 152–158.

Libowitzky E. (1999) Correlation of O–H stretching frequencies and O–H···O hydrogen bond lengths in minerals. *Monatshefte für Chemie*, **130**, 1047–1059.

Öhman L., Nysten P. and Langhof J. (2004) Famous mineral localities: the Bastnäs mines – Riddarhyttan ore field, Bergslagen district, Västmanland, Sweden. *Mineralogical Record*, **35**, 187–200.

Pasero, M. (2020) *The New IMA List of Minerals.* http://cnmnc.main.jp/

Pekov I.V., Alimova A.N., Kononkova N.N. and Kanonerov A.A. (2002) On the mineralogy of Mochalin Log at Southern Urals I. Minerals of the bastnäsite family: history of studies and new data. *Uralskiy Geologicheskiy Zhournal (Uralian Geological Journal)*, **4**(28), 127–144 [in Russian].

Sheldrick G.M. (2008) A short history of *SHELX. Acta Crystallographica*, **A64**, 112–122.

Silberminz V.A. (1928) The primary deposit of cerite in Kyshtym district. *Mineral'noe syr'e* (*Mineral Raw Materials*), **9/10**, 619–620 [in Russian].

Silberminz V. (1929) Sur le gisement de cerite, de bastnäsite et d'un minéral nouveau la lessingite dans le district minier de Kychtym (Oural). *Comptes Rendus de l'Academie des Sciences de Russie*, A, **3**, 55–60 [in French].

Silberminz V.A. (1930) The deposit of cerite in Kyshtym district (Urals) Pp. 5–42 in: *Rare-Earth Minerals of Kyshtym Area. Trudy Instituta prikladnoy mineralogii* (*Proceedings of the Institute of Applied Mineralogy*), **44** [in Russian].

Svyazhin N.V. (1956) Primary deposits of rare-earth and rare-metal minerals of Mochalin Log, Kyshtym district, Chelyabinsk Oblast. *Trudy*

Sverdlovskogo Gornogo Instituta (Works of the Sverdlovsk Mining Institute), **28**, 88–98 [in Russian].

Svyazhin N.V. (1962) Törnebohmite from alkaline province of Urals. *Zapiski Vsesoyuznogo Mineralogicheskogo Obshchestva*, **91**, 1, 97–99 [in Russian].

Svyazhin N.V. (1965a) New data on lessingite. Pp. 239–244 in: *Minerals of Ore Deposits and Pegmatites of Urals. Trudy Instituta geologii Uralskogo filiala AN SSSR (Proceedings of the Institute of Geology of the Uralian Branch of AS of USSR)*, **70** [in Russian].

Svyazhin N.V. (1965b) Kyshtymite as a bastnäsite variety. Pp. 249–252 in: "*Minerals of ore deposits and pegmatites of Urals*". *Trudy Instituta geologii Uralskogo filiala AN SSSR (Proceedings of the Institute of Geology of the Uralian Branch of AS of USSR)*, **70** [in Russian].

Yunikov B.A. and Svyazhin N.V. (1965) X-ray study of cerite. Pp. 245–247 in: *Minerals of Ore Deposits and Pegmatites of Urals. Trudy Instituta geologii Uralskogo filiala AN SSSR (Proceedings of the Institute of Geology of the Uralian Branch of AS of USSR)*, **70** [in Russian].